Project Number: ME-CAB-1702

Analysis of Edge Curvature and Roughness in Slicing

A Major Qualifying Project Report:

Submitted to the Faculty of the

WORCESTER POLYTECHNIC INSTITUTE

In partial fulfillment of the requirements for the

Degree of Bachelor of Science

By

____

Jake Porrazzo (ME)

____

Michael Sheahan (ME)

____

Scott Spear (ME)

Date: April 25, 2017

Approved:

____

Professor Christopher A. Brown
Major Advisor

Abstract

The objective of this project is to investigate the strength of the correlations between the finish along an edge to the edge geometry and performance when slicing through a given material. We used a state of the art microscope to measure machined aluminum edges at fine scales. We used geometric multiscale analyses to characterize the edge and determine the relevant scales of measurement. We redesigned a testing device from a previous MQP to apply measurable forces when slicing through material. We used a dynamometer to measure the forces simultaneously. Using the microscope to analyze the edges before slicing, as well as the material after slicing, it was determined that various polished edge finishes resulted in differences in slicing performance. However, there were no strong correlations discovered between relative area and curvature at any scale. There were correlations found between curvature and complexity at higher scales, 10^4µm to 10^5µm, but this could be due to noise in our measurements.

Table of Contents

Table of Figures

Acknowledgements

We would like to thank the following people for their contributions to our project:

Professor Christopher A. Brown

Adam J. Frewin

Matthew A. Gleason

WPI Surface Metrology Laboratory Staff

WPI Library Staff Members Paige Neumann and Lori Steckervetz

1. Introduction

1.1 Objective

The objective of this project is to investigate the strength of the correlations between the finish along an edge to the edge geometry and performance when slicing through a given material.

1.2 Rationale

There is currently no universal method for measuring the sharpness of an edge. Various studies have conducted research and experiments that propose methods of measuring how sharp an edge is, but none have been universally adopted. The sharpness of an edge has effects on food preparation, food packaging, and food processing, as well as medical practice and examination.

Processing, preparing, and packaging food can experience critical downtimes in production when tools and cutting instruments need to be sharpened. The wear on a sharp edge effects the frequency of the downtimes, making the maintenance of sharp edges vital. Slicing deli meat, filleting fish, and cutting vegetables are examples of common actions involving the slicing of material with sharp edges. In a 2003 study, blade sharpness was found to affect grip forces, cutting time, and cutting moments more than dull knives in lamb shoulder boning and beef rib trimming (McGorry et al., 2003).

Medical practices such as surgeries and examinations often require “high” sharpness of the surgical instrument edges. In the case of slicing flesh for surgery, the sharper blades are used for faster and cleaner cutting, but also aid in speeding up the healing process of the incision, and minimizing the scarring of the incision (Tsai et al., 2012). Different medical procedures also require different degrees of sharpness, much like in the case of corneal surgery, where extremely high sharpness is used to make the most precise and clean incisions (Viestenz et al., 2003).

Slicing is important in the skiing industry. Skiing is a growing industry with over 115 million skiers worldwide (Korecki et al., 2016). Ski blades are sharpened with edges that are meant to carve into the skiing surface enough to prevent skidding when carving a turn (Wilson, 2003). When the sharpness of ski edges is compromised, they are often taken to ski shops for tuning, which is costly for the skier. Providing a solution to the frequent dulling of ski edges can allow for longer ski outings, less downtime, and better performance.

1.3 State of the Art

1.3.1 Measuring Sharpness

There exists no current measurement for the sharpness of a blade (McGorry et al., 2003). Some of the most common measurements observed in cutting and slicing are cutting time, peak cutting moment, mean cutting moment, grip forces, and number of cuts, primarily (McGorry et al., 2003). By developing a range for each of the above measurements, the sharpness of an edge can be gauged (McGorry et al., 2003). There are also no commercially available devices that can explicitly measure the sharpness of an edge (McGorry et al., 2003).

In 2007, a study was conducted that developed the Blade Sharpness Index (BSI) that is represented in the following formula (McCarthy et al., 2007).

$$BSI = \frac{2A\delta_i^2 + 2B\delta_i}{6tJ_{IC}}$$

δ_i = blade displacement

t = time

J_{IC} = fracture toughness

A and B are empirical constants

The blade displacement δ_i is measured using a 50 kN Tinius-Olsen universal testing machine (McCarthy et al., 2007). The fracture toughness J_{IC} is defined as the material's resistance to fracture (McCarthy et al., 2007). The BSI and cutting force relate directly to the tip radius of the edge of the cutting instrument (McCarthy et al., 2007). The tip radius is shown in the figure below, along with the wedge angle of the edge, and a graph of the relationship between the tip radius, BSI, and force at cut formation.

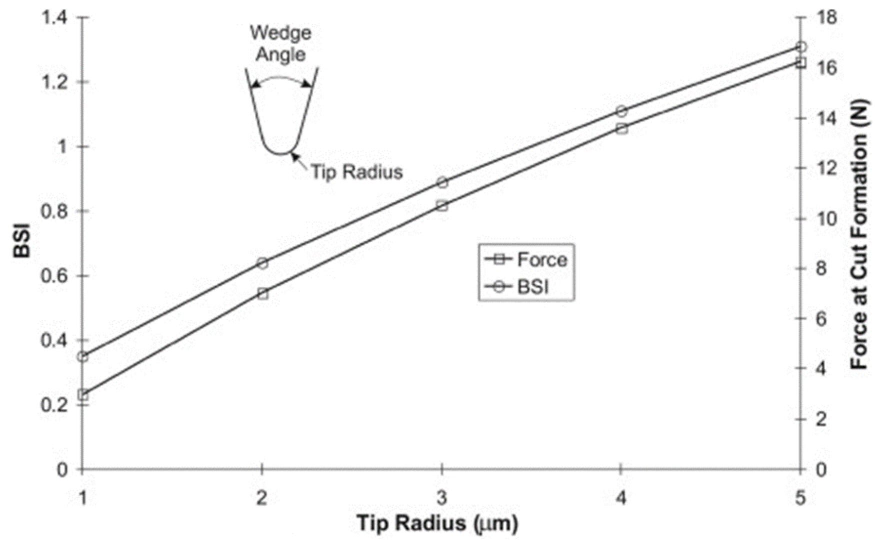

Figure 1: Tip Radius vs. BSI and Force at Cut Formation (McCarthy et al., 2007)

The BSI can be calculated from knowledge of the tip radius, and it is also possible to use the wedge angle as opposed to the tip radius (McCarthy et al., 2007). Figure 2 shows the correlation between the wedge angle, BSI, and cutting force (McCarthy et al., 2007).

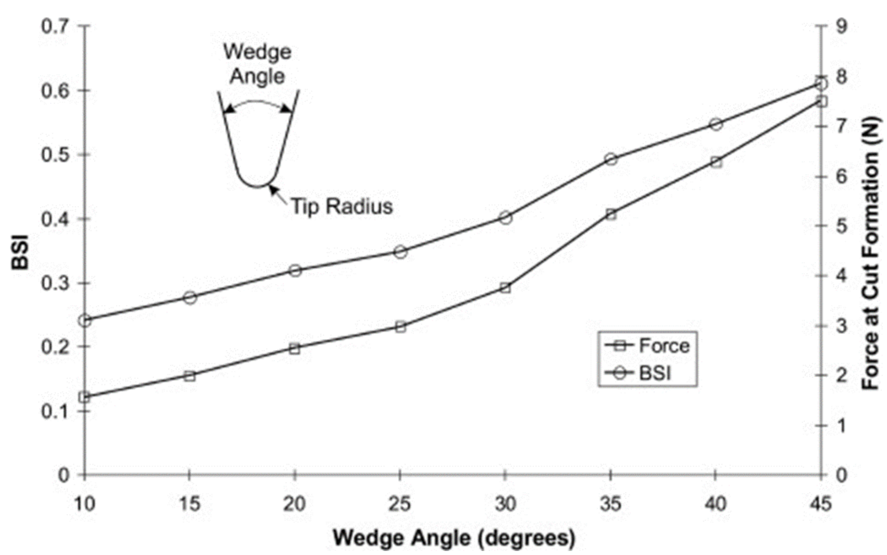

Figure 2: Wedge Angle vs. BSI and Force at Cut Formation (McCarthy et al., 2007)

Analyzing Figure 2, it is observed that an increased wedge angle is present in a less sharp edge and the force at cut formation is also increased.

1.3.2 Slicing

The sharpness of the edge of a ski blade affects the performance of the ski slicing through a turn. During the carving or slicing of a turn, the "cutting" force is directed at oblique angle to the skiing surface. The two forces acting on the ski edge are the tangential, or horizontal centrifugal, and normal, or downward, forces. There is equal force exerted from the skiing surface, allowing the ski to carve into the turn based on the sharp edges which prevent skidding downward. Newton's Third Law allows the skier to slice into the surface and carve a turn, as opposed to skidding and scraping down the slope (Wilson, 2003).

There are two angles that are most prominent in the mechanics of carving a turn, being the dig angle and the skid angle. The dig angle is the acute angle between the blade and the skiing surface which is in the direction of the turn, resulting in force generated in the opposite direction of the turn. The skid angle is the acute angle between the blade and the skiing surface in the opposite direction of the turn, resulting in force generated in the direction of the turn. These angles determine the balance of the forces on the contact surface of the ski edge and distribute the forces accordingly (Wilson, 2003).

1.4 Approach

1.4.1 Axiomatic Design

Using axiomatic design, we adapted a testing apparatus that yielded results on the effects of various tip radii on the forces necessary to produce a slice in a material. The main goal of the axiomatic design was to decouple the vertical and horizontal forces acting upon the cutting instrument by using compressed air to gauge the horizontal force and a weight to provide the vertical force. A dynamometer is used to measure both of these forces simultaneously. The design incorporates some of the functionality present in previous work on scraping in skiing quasi-statics, and advances the state-of-the-art by universalizing a testing method for the sharpness of a blade or edge with measurable force in the x and y directions. The main point of emphasis was to limit any motion other than in the z and y directions, and to measure the forces.

#	[FR] Functional Requirements	[DP] Design Parameters
0	Measure slicing performance of a blade	Device that allows edge to slice through material
1	Measure force applied to material	Dynamometer
1.1	Measure the normal force	Dynamometer clamp for sliced material
1.2	Measure horizontal force	Piezoelectric crystal dynamometer for multi-axis
2	Restrict upwards vertical movement	Pneumatic cylinder
2.1	Constant downard force	Pneumatic pressure line
2.2	Measure vertical propellant forces	Pressure gauge
3	Restrict horizontal movement along one axis	Linear bearings
3.1	Contant force to move blade in one axial direction	Pneumatic pressure parallel to linear bearing axis
3.2	Measure horizontal propellant forces	Pressure gauge
4	Fix blade to device	Blade clamping fixture
4.1	Align corect height over material	Spacers connected to linear bearing rails
4.2	Hold device for stability	Clamps
4.2.1	Restrict lateral movement	Side plate
4.2.2	Restirct resistive movement on horizontal axis	Back plate
4.2.3	Lock blade in place	Screw with knurled knob
5	Fix material to dynamometer	Bolts
5.1	Stablize dynamometer	Countersunk bolts in base
5.2	Align dynamometer with material	Clamping system
5.2.1	Restrict material movement in horizontal direction	Metal block at end of dynamometer
5.2.2	Restrict upward vertical movement of material	C-clamps

Figure 3: Axiomatic Design of Testing Apparatus

1.4.2 Measurements of Tip Radius and Depth of Cut

Utilizing the Olympus LEXT OLS4100 laser scanning confocal microscope, we are focusing on measuring elevations on the edge, and using Heron's formula to evaluate and identify the curvature of the tip of the edge. Additionally, the confocal microscope is compatible with the MountainsMap software, which allows us to analyze the roughness profile and parameters. The measurements imported from the microscope to the MountainsMap software will yield the tip radius, which we are investigating the correlations with performance of cut.

Further measurements from the confocal microscope and MountainsMap software will include the depth of cut of the paraffin wax after experimenting with the testing apparatus. Following a similar procedure as the measurement of the edge, we will be examining the profile of the cut in the wax, and relating the profile of the cut to the tangential and normal forces necessary for cut formation. Analyzing and comparing the depth of cut and force at cut formation from the testing apparatus, coupled with the measurements from the Olympus confocal microscope will present us with the quantitative data necessary for correlation investigation and graphical representation of the independent and dependent variables.

1.4.3 Force Measurements using Kistler Dynamometer

The testing apparatus that we developed from SolidWorks drafting and mill machining will be used in tandem with a Kistler Dynamometer, fitted with a piezoelectric crystal to measure the tangential and normal forces during cut formation. The dynamometer will emit voltage representations of the forces, and with LabVIEW software, we will be able to convert the voltage measurements into force measurements. Using LabVIEW software, we will be able to distinguish the force measurements of varying edges for further analysis. These measurements will be incorporated with profile measurements from the confocal microscope to develop graphical representations of the roughness profiles, curvature, and necessary force for cut formation.

2. Methods

2.1 Curvature Measurements

Measurements of the surface roughness and curvature of each aluminum edge were recorded using the Olympus LEXT 4100 laser scanning confocal microscope in the Surface Metrology Laboratory at WPI. To measure the surface roughness of the aluminum edges, the aluminum was placed on the microscope base as shown in the figure below. The microscope was then focused at each magnification (5x, 10x, 20x, 50x high standoff) until reaching the target magnification of 50x low standoff to capture the surface roughness at an appropriate resolution. The low standoff of the 50x microscope was used to minimize the reflection of light from the aluminum edge, which would affect the topographical measurements and images being scanned.

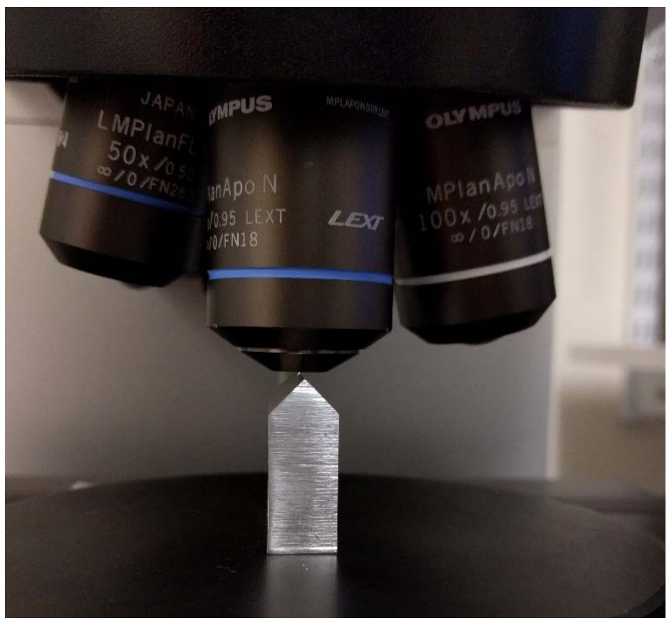

Figure 4: Edge on Microscope

In order to test the performance of varying tip radii for aluminum edges under a load, a testing apparatus was developed using the principles of axiomatic design. To measure the critical forces at cut formation as applied by the normal and tangential air pressure, a Kistler dynamometer was incorporated on the bottom of the frame, underneath the wax being sliced. After attaching the dynamometer to the National Instruments Data Acquisition Box (DAQ box) provided by the Engineering Experimentation Laboratory at WPI, the National Instruments LabVIEW software was run to capture the voltage data emitted from the dynamometer and through the DAQ box during dynamic testing. The LabVIEW software converted the piezoelectric crystal voltage readings from the dynamometer into interpretable force readings, measuring precisely the tangential and normal forces during the slicing motion of the aluminum edge.

In order to analyze the data from LabVIEW, the measurements were exported to Microsoft Excel, where they could be easily organized in graphs. The graph that was developed for each measurement was a load versus time graph, where the tangential and normal loads were plotted over time respectively. This type of graph was chosen because the critical force at cut formation would be the highest force reading on the graph, showing a precise point in time where the aluminum edge broke the critical boundary of stiffness and began slicing the wax.

2.1.1 Materials

The material chosen for slicing performance of the aluminum edges was paraffin wax because the properties of the wax limit elastic deformation. The wax also has the ability to hold the shape of a cut at room temperature for observation under the microscope.

2.1.1.1 Edge Preparation

To prepare the aluminum edges, we used CNC machining. For the CAM operations, Esprit was used. The program was then uploaded to a Haas Mini Mill for machining. Below is an image of the CAM simulation of what the edge was supposed to look like after the operation was complete.

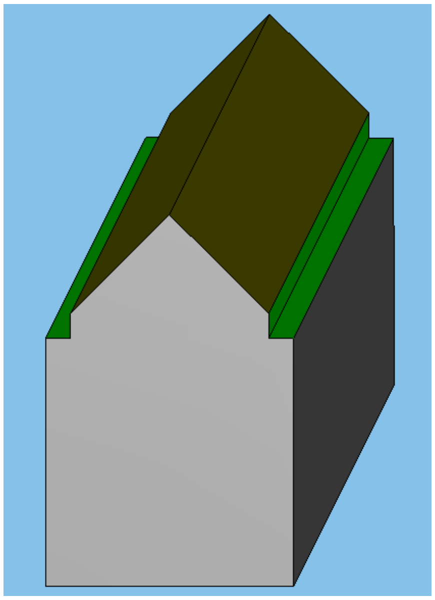

Figure 5: Edge Trial 1 CAM Operation, Edge Dimensions: 0.5x1.0x1.25in (ESPRIT CAM*)*

We initially tried this method for the edges. The step was put in the sides to allow for a ⅜ drill mill to create a 90 degree edge because the cutting radius on this tool is only 0.375in, and our stock was 0.5in. This method worked in the machining phase, but caused problems when it came to polishing the edges. We were planning on polishing the edges using different polishing finishes from different sandpaper grits and mass finisher times. We preliminarily polished these edges by hand, in a direction perpendicular to the tip of the edge. This proved to be an ineffective method, especially with the step. The edge of the step would interfere with the polishing of the tip edge we were trying to measure, and the perpendicular polishing would cause a burr and an uneven polish.

To get a better edge, the next machining operation included facing material off the bottom, so the edge would lay flat while on the microscope, and facing off 0.125in of the 0.5in stock on the sides, so the total width would be 0.375in, which is the same size as the cutting radius of the tool we used. This eliminated the need for the step to be created for the cutting length of the drill mill. Below is an image of this new operation.

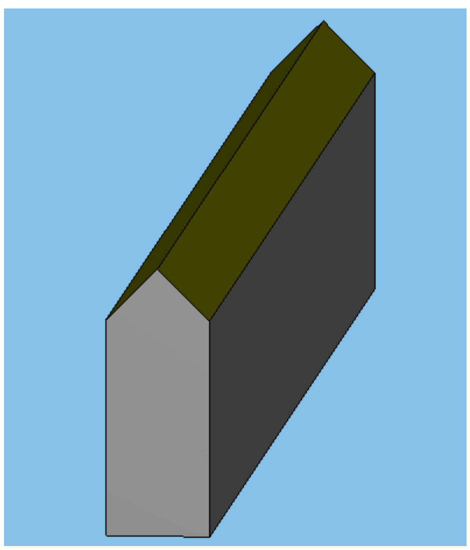

*Figure 6: Edge Trial 2 CAM Operation, Edge Dimensions: 0.375x1.0x1.25in (*ESPRIT CAM*)*

Once the operation was complete, we noticed that there was a small flat on the top where there was supposed to be a perfect 90 degree tip. There could have been a number of reasons this occurred. On the 90 degree drill mill used for the operation, there was a 0.03125in flat on the very tip of the tool. If this offset was not correctly programed the tool would have been offset by this amount, causing a flat. A chip in the tool is another possibility for the operation to not be correct. A chip would have caused the tool to not make contact at the instance when the chip passed over the material.

To correct this, the edge was brought to a Bridgeport Manual Mill and set onto a 45 degree vice. With a ⅝ end mill, we dropped the total depth down by 0.01in. We then flipped the piece around and ran it through again. This cleaned up the small flat and brought the edge to 90 degrees. Below is an image of the setup for the manual milling.

Figure 7: Aluminum Edge on 45 Degree Vice on Manual Mill

This manual machining left us with a rather rough machine finish and a large burr along the edge. Below is an image of the machine finish on the edge.

Figure 8: Unfinished Edge, Edge Dimensions: 0.375x1.0x1.25in

This time to polish the edges, we designed and machined a fixture to hold the edge during polishing. This fixture allowed us to make sure there was an even polish across the edge. We also polished the edges parallel to the edge tip to avoid causing a burr and uneven polishing.

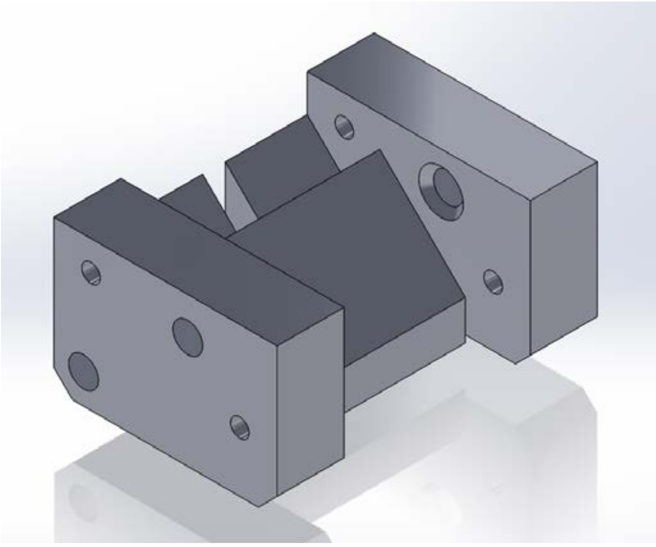

*Figure 9: Solidworks Model of Polish Fixture with Edge, without ¼-20 SHCS and Dowels (*SolidWorks*)*

To setup the polish fixture, we placed the two halves of the fixture on 0.01in feeler gauges, which we placed on a granite surface plate to ensure the fixture was level. We then placed the edge on the angled part of the fixture, so the edge to be polished was lying flat on the granite, and then tightened the fixture. See image below for the polish fixture setup.

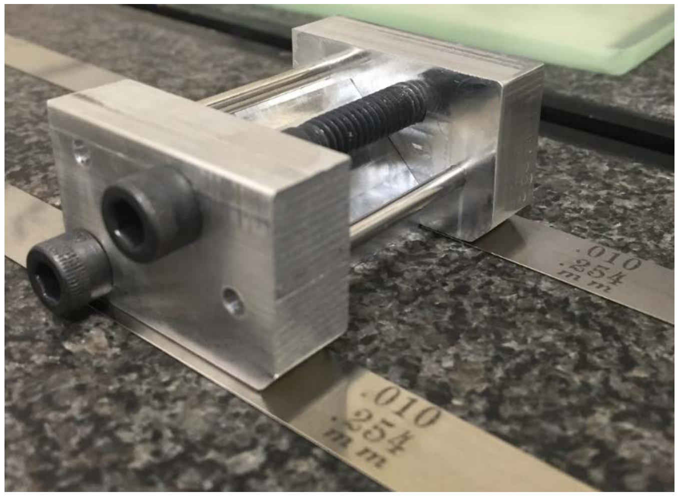

Figure 10: Polish Fixture Setup with Edge, Edge Dimensions: 0.375x1.0x1.25in

Four edges were polished using 1200, 1500, 2000, and 3000 grit polish paper for aluminum. Three separate edges were polished to 3000 as well, and then placed separately in the mass finisher for 2, 4, and 8 minutes.

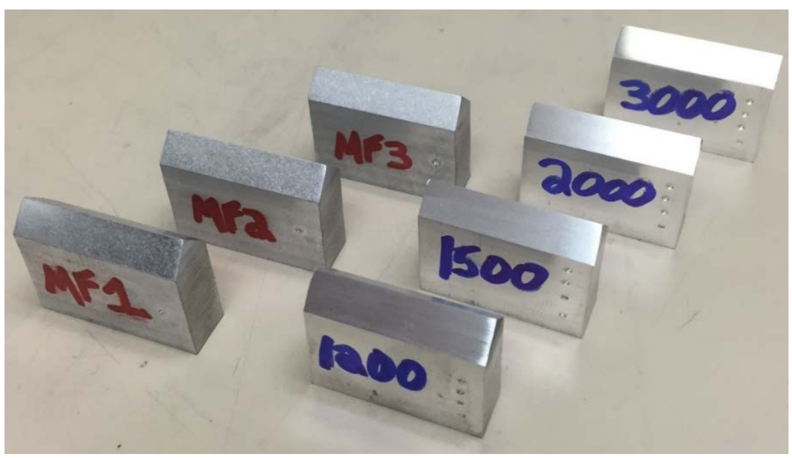

Figure 11: Finished Edges Ready for Testing, Edge Dimensions: 0.375x1.0x1.25in

2.1.1.1.1 Unfinished Edge

The first edge we measured was the unfinished (machined) edge. It is evident in the images below that this caused a large burr and a rough finish. These images below are of both a 3D and 2D topographic plot of the edge tip. All of the edges were measured using the 50x low standoff lens on the Olympus microscope. The 3D figure shows the isometric view of the image produced from microscope. The 2D figure shows the size of the burr relative to the rest of the edge.

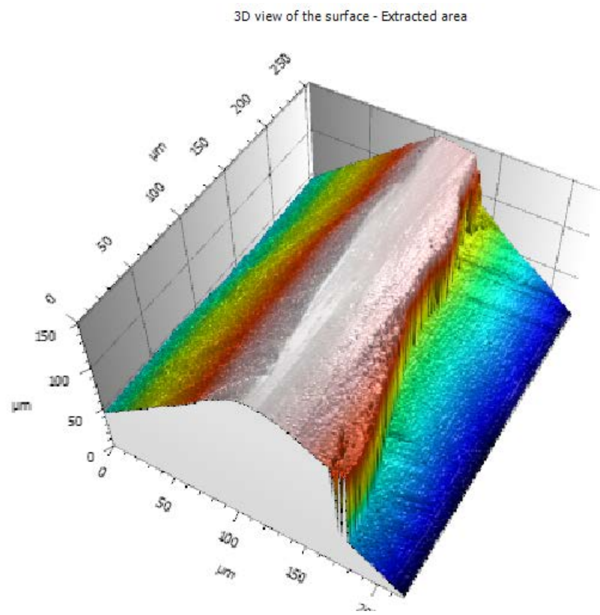

*Figure 12: 3D Elevation Profile of Unfinished Edge (*MountainsMap*)*

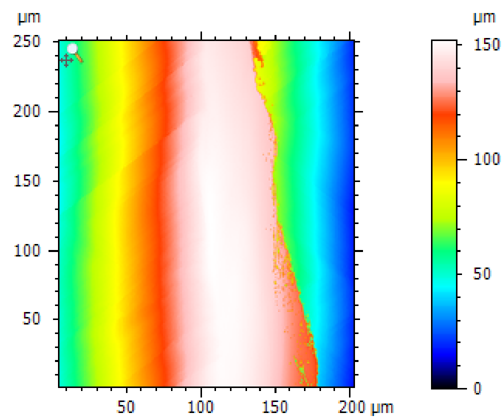

*Figure 13: 2D Elevation Profile of Unfinished Edge (*MountainsMap*)*

2.1.1.1.2 Polished Edge- 1200 Grit

The first edge we polished was polished using a 1200 grit polish paper for aluminum. As you can see from the figure below, by polishing the edge, you remove the burr and create an even surface. The 1200 grit was the roughest grit paper we used, which you can see by the larger ridges on the sides of the edge. You can also see the direction of the polishing was parallel to the tip of the edge.

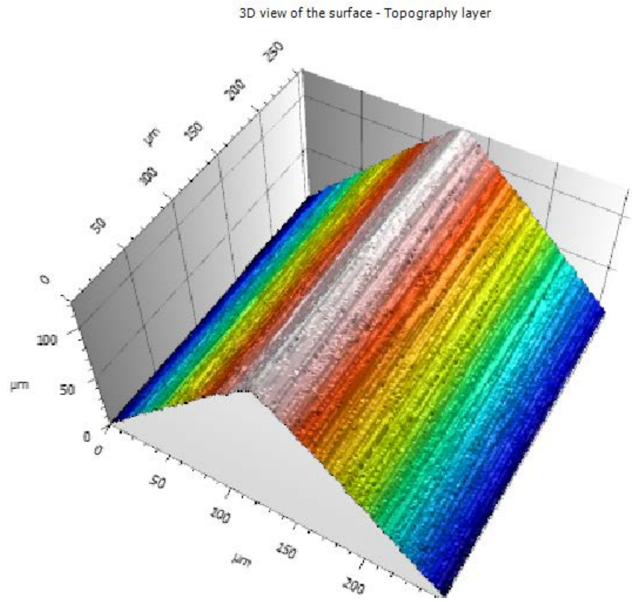

*Figure 14: 3D Elevation Profile of 1200 Grit Polished Edge (*MountainsMap*)*

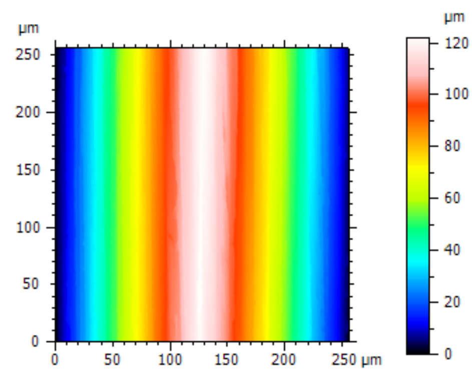

*Figure 15: 2D Elevation Profile of 1200 Grit Polished Edge (*MountainsMap*)*

2.1.1.1.3 Polished Edge- 1500 Grit

The next polish we used was a 1500 grit polish paper. As you can see from the images below, it creates a bit of a finer finish on the edge. The size of the ridges on the edge are smaller than those of the 1200 grit. The ridges are still quite visible however.

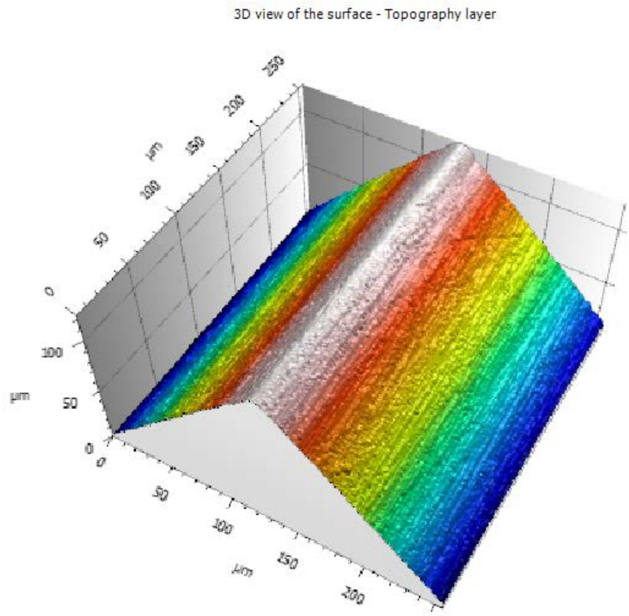

*Figure 16: 3D Elevation Profile of 1500 Grit Polished Edge (*MountainsMap*)*

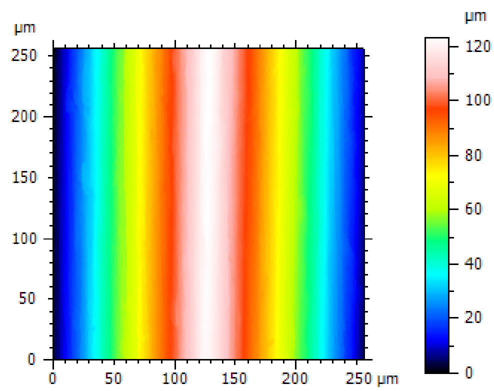

*Figure 17: 2D Elevation Profile of 1500 Grit Polished Edge (*MountainsMap*)*

2.1.1.1.4 Polished Edge- 2000 Grit

Next, we used a 2000 grit polish paper. This becomes an even smoother finish. The size of the ridges are smaller than those of the 1200 and 1500 grit finishes. The tip of the edge is cleaner and comes to a more fine point.

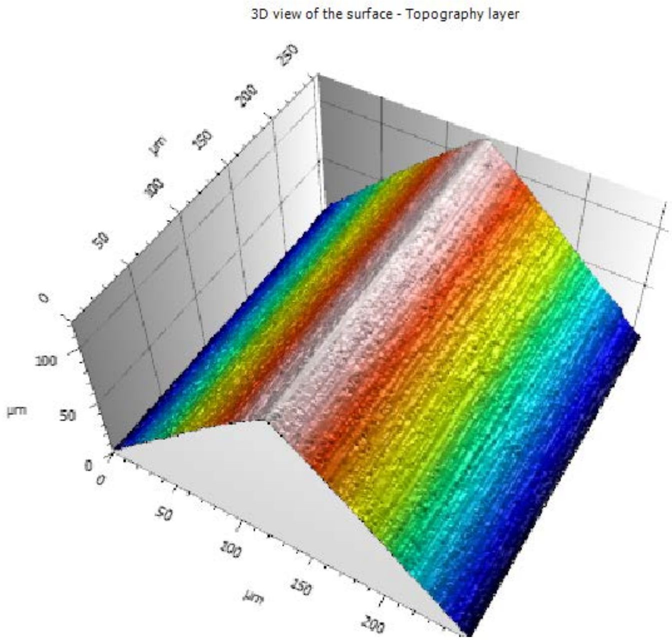

*Figure 18: 3D Elevation Profile of 2000 Grit Polished Edge (*MountainsMap*)*

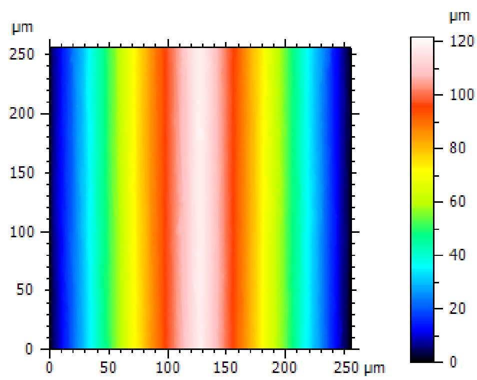

*Figure 19: 2D Elevation Profile of 2000 Grit Polished Edge (*MountainsMap*)*

2.1.1.1.5 Polished Edge- 3000 Grit

The final polish we used was a 3000 grit polish paper. This created the smoothest finish, which was expected. The ridges that were clearly visible in the 1200, 1500, and 2000 grit polishes are almost completely gone. There is a clear point to the tip of the edge, and what cannot be seen in this image is that there is a mirror finish. This only happened with the 3000 grit polished edge. The other edges were close to mirror finish, but with the 3000 grit, it was very distinguishable.

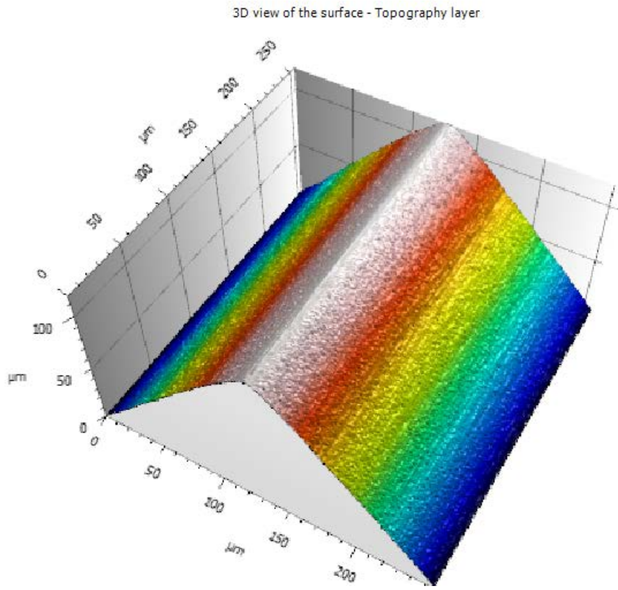

*Figure 20: 3D Elevation Profile of 3000 Grit Polished Edge (*MountainsMap*)*

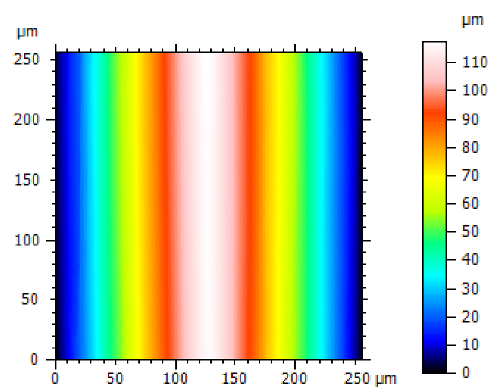

*Figure 21: 2D Elevation Profile of 3000 Grit Polished Edge (*MountainsMap*)*

2.1.1.1.6 Mass Finished Edge- 2 Minutes

The next set of edges we prepared were polished up to the 3000 grit polish paper and then placed in the mass finisher for a set period of time. This edge was mass finished for two minutes. As you can see in the images below, the fine pointed edge that the 3000 grit polish created was rounded out by the mass finisher. It also created a rougher surface than the polished edges. The ridges that were evident in the polished edges do not reappear, but the finish seems to be covered with crater looking imperfections. They appear mostly on the rounded tip of the edge.

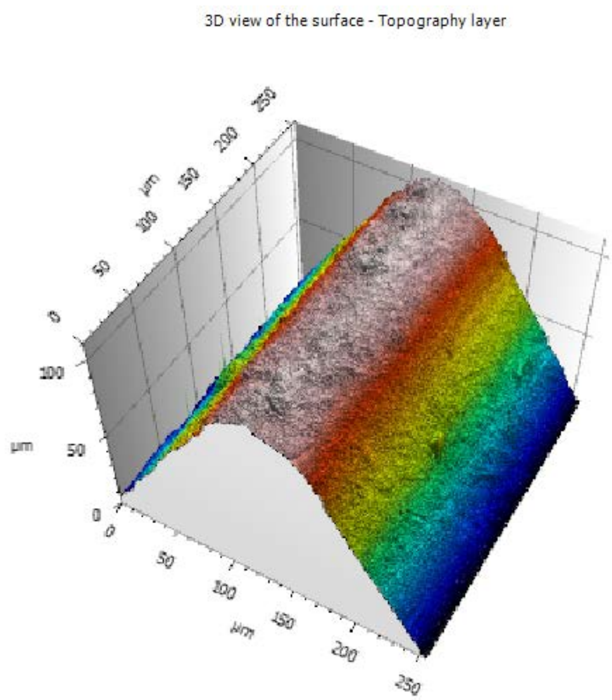

*Figure 22: 3D Elevation Profile of 2 Minute Mass Finished Edge (*MountainsMap*)*

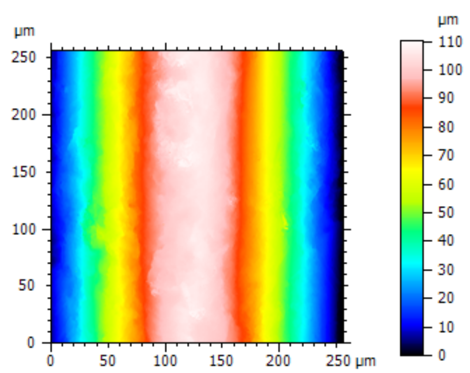

*Figure 23: 2D Elevation Profile of 2 Minute Mass Finished Edge (*MountainsMap*)*

2.1.1.1.7 Mass Finished Edge- 4 Minutes

The next edge was placed in the mass finisher for four minutes. It is clear that the tip of the edge became more rounded than that of the two minute mass finished edge. The crater-like imperfections seem to be greater in number and in size along the tip of the edge.

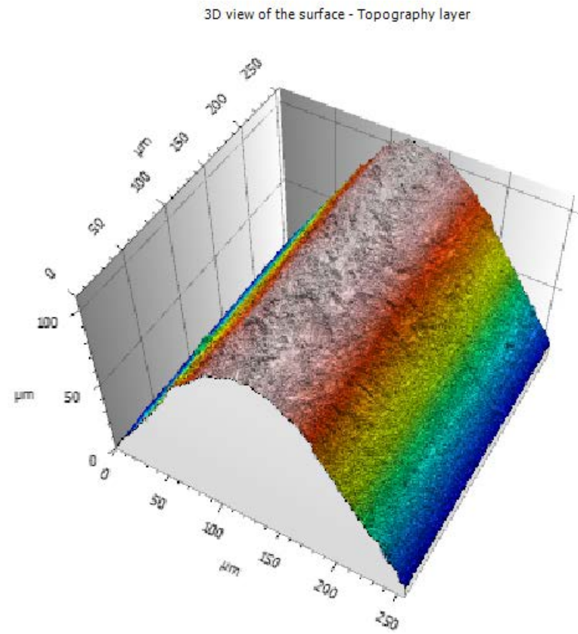

*Figure 24: 3D Elevation Profile of 4 Minute Mass Finished Edge (*MountainsMap*)*

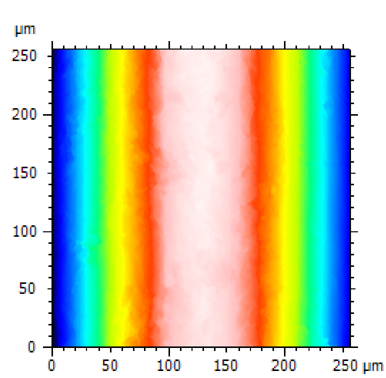

*Figure 25: 2D Elevation Profile of 4 Minute Mass Finished Edge (*MountainsMap*)*

2.1.1.1.8 Mass Finished Edge- 8 Minutes

The final edge was placed in the mass finisher for eight minutes. The rounded edge became even more rounded, and the imperfections became greater in size and number again.

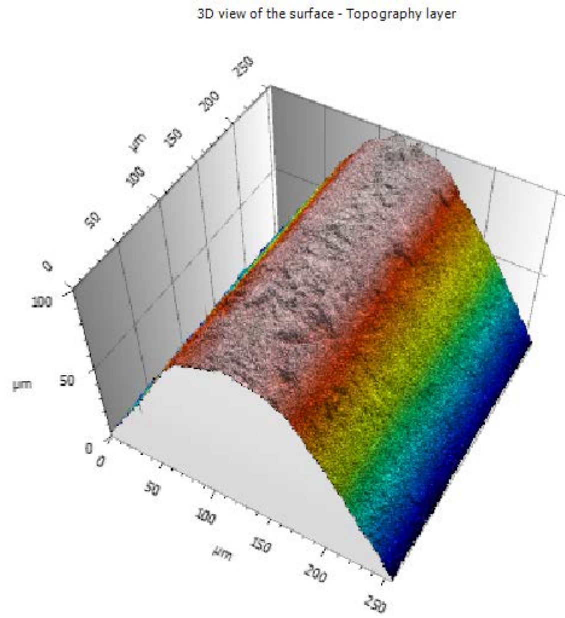

*Figure 26: 3D Elevation Profile of 8 Minute Mass Finished Edge (*MountainsMap*)*

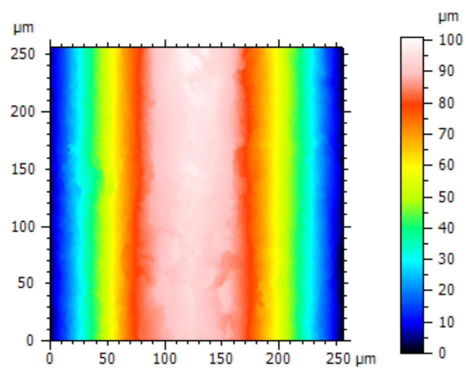

*Figure 27: 2D Elevation Profile of 8 Minute Mass Finished Edge (*MountainsMap*)*

Please refer to Appendix D for more information.

2.1.1.2 Wax Preparation

To prepare the wax for cutting, we created a mold to form it into smaller rectangular blocks to fit into our material fixture during the slice testing. We created the mold using Solidworks 3D modeling software, and then used 3D printing to manufacture the mold itself. We chose to use additive manufacturing for this because it was cheap and could be made quickly. The ABS plastic is also more elastic than metals, so it would be easier to get the wax out once it was completed. Below is an image of the Solidworks model for the mold.

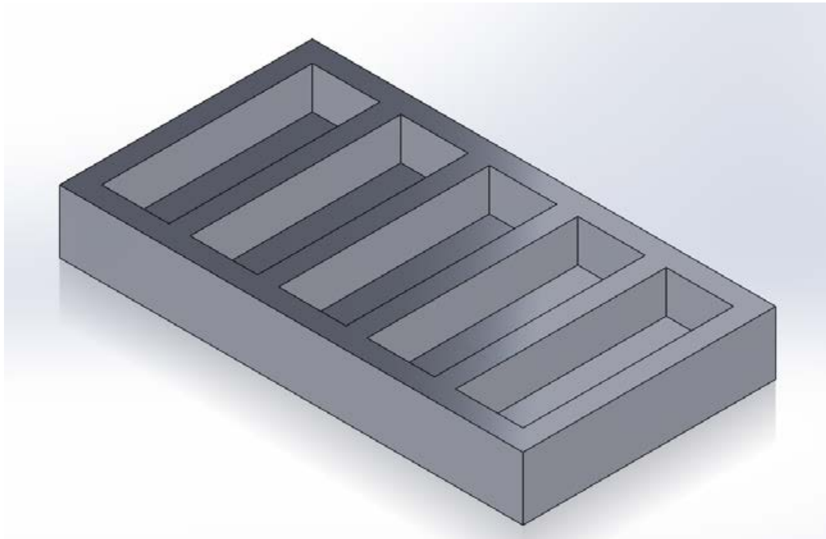

Figure 28: Solidworks Model of Wax Mold (SolidWorks)

We melted the wax by double boiling it. We boiled water in a large pot, and then placed a bowl on top of the pot. This technique prevents the wax from being exposed to open flame, which could cause the wax to burn and adhere to the sides of the pot. The wax was then poured into the mold and placed in the freezer to harden.

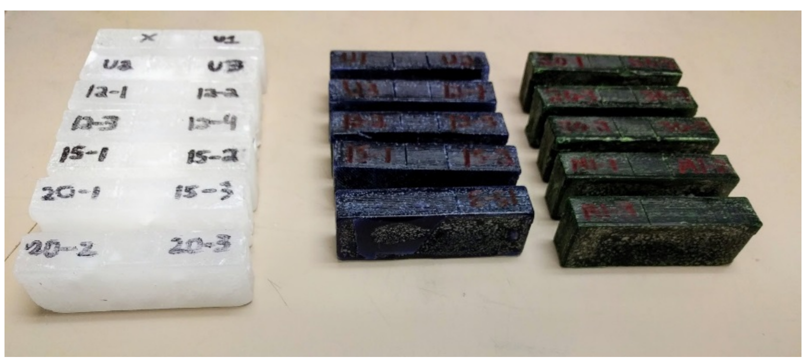

Figure 29: Wax Blocks after Slicing, Wax Dimensions: 0.375x0.5x2.0in

After initial testing and observation of the wax under the microscope, it was determined that the white colored wax was allowing too much light through during scanning of the laser. We fixed this by adding wax coloring that is used to make colored candles. While the wax was melted, we added blue coloring to one set of edges and green coloring to another. These darker colors made the wax more opaque, which helped while measuring the slice under the microscope because it allowed less light to travel through the wax.

2.1.2 Calculation

For the curvature calculations, we will be utilizing Curvsoft, which is a curvature program created by students at WPI. The program uses Heron's formula to calculate the curvature of an edge. If the edge is less than 90 degrees, the software uses a hybrid calculation of Heron's formula and the calculus derivative method to calculate curvature. In our case, the edges are approximately 90 degrees, therefore the calculations will be solved using Heron's. This formula calculates the curvature by solving for the area of the triangle from the three points selected to define the edge.

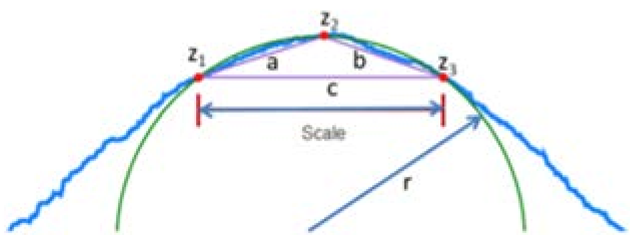

$$s = \frac{a+b+c}{2} \quad (1)$$

$$h = \sqrt{s(s-a)(s-b)(s-c)} \quad (2)$$

$$k_h = \frac{1}{r} = \frac{4h}{a*b*c} \quad (3)$$

Figure 30: Definition of the Points on a Profile for Calculation of Curvatures (Gleason et al., 2013)

2.2 Force Measurements

2.2.1 Testing Apparatus

The majority of the testing apparatus was made by a previous MQP team, which was focused on the scraping aspect of cutting, and then also adapted for a project in which the team was testing the correlation of coefficient of friction with different sole materials in shoes. Our team took this device and modified it to fit our slicing needs.

2.2.1.1 Edge Fixture

The first part we needed to make was a fixture to hold our edges during slicing. The fixture needed to be fixed to the air cylinder to allow for vertical movement. This was accomplished with a ¼-28 threaded hole in the top of the fixture to screw the air cylinder threaded rod into. We needed to ensure there would be no rotational movement in the edge during slicing because we needed a perfectly straight cut. We used two locating dowels to ensure no rotational movement occurred. We used a knurled knob, a threaded rod, and a cylinder with a threaded hole in the middle to hold the edge in the fixture. There was a threaded hole placed in the center of one of the sides of the fixture to allow for this.

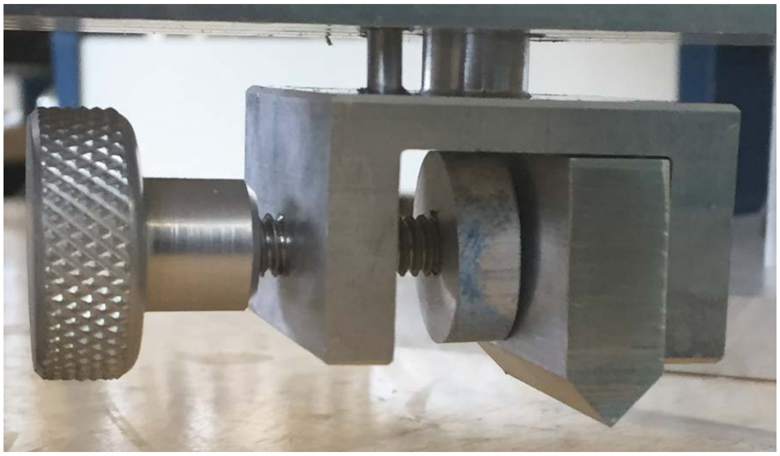

Figure 31: Edge Fixture with Edge

Please refer to Appendix B for Solidworks models and CAM simulations of operations.

2.2.1.2 Material Fixture

The next part we needed to create was a fixture to hold the wax in place during slicing. The fixture needed to be secured to the dynamometer to prevent the fixture from moving. The dynamometer comes with M8 threaded holes on the top surface. We created a fixture with slots to accommodate these M8 screws.

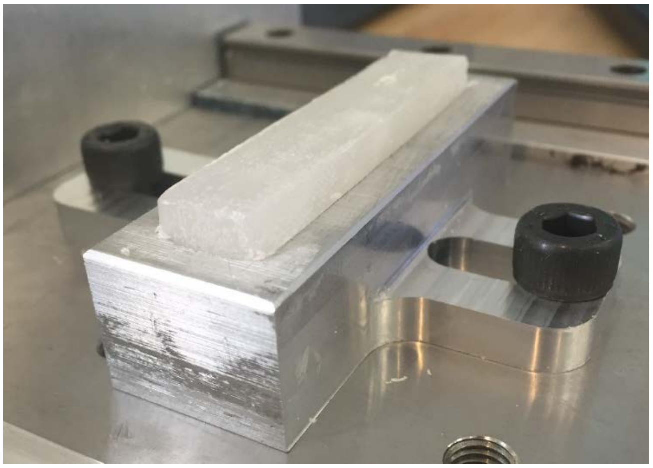

Figure 32: Material Fixture with Wax Block

Please refer to Appendix B for Solidworks models and CAM simulations of operations.

2.2.1.3 Locating Dowel Holes in Top Slide

The rail that runs on the linear bearings was already machined by a previous group. The only modification we had to make were the two guide holes for the locating dowels.

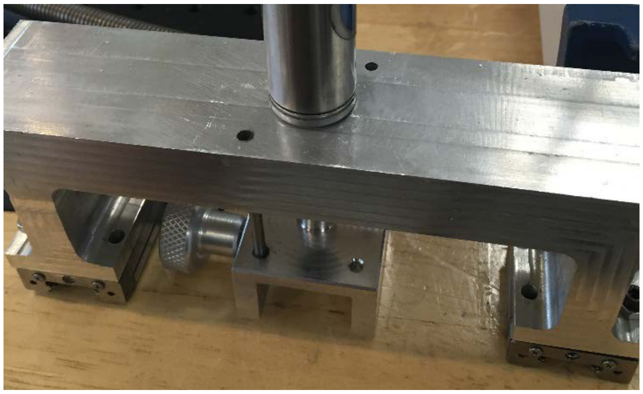

Figure 33: Sliding Rail with Dowel Guide Holes and Air Cylinder

Please refer to Appendix B for Solidworks models

2.2.1.4 Spacers

Because of the size of the material fixture and the edge fixture, the linear bearings need to be raised up 0.75in to allow for clearance of the edge and the wax. This was completed by taking aluminum stock cut to the desired size and drilling two threaded holes and two counter bored holes into the top surface. The counter bored clearance holes were used to sit the bolts, which held the spacers down to the bracket already made, flush with the top surface so the linear bearing rails would lay flat. The threaded holes were to bolt the linear bearing rails down to the spacers. We also needed to drill and tap holes into the existing bracket to hold the spacers down. The figure below shows the setup, along with numbers that correspond to their decomposition numbers in the axiomatic design.

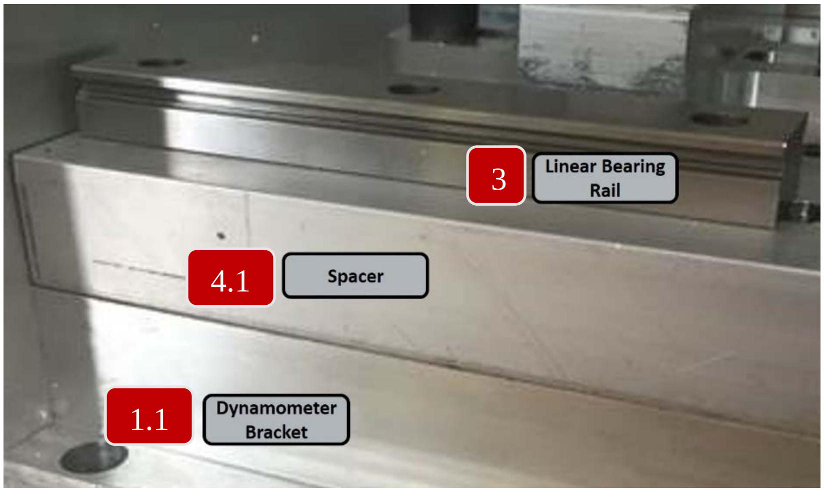

Figure 34: Spacer with Linear Bearing Rail

Please refer to Appendix B for Solidworks models and CAM simulations of operations.

2.2.1.5 Back Plate

There was an existing plate to hold the horizontal air cylinder, but since we added the spacers to the apparatus, this air cylinder needed to be raised as well. Unfortunately, we could not just add a hole higher up on the existing plate because it was not tall enough. We took a larger piece of stock and machined new slots to resemble the existing slots and drilled and tapped a ½-20 threaded hole higher on the plate to accommodate the new location of the sliding rail.

Figure 35: Back Plate with Horizontal Air Cylinder

Please refer to Appendix B for Solidworks models and CAM simulations of operations.

2.2.2 Dynamometer

To measure forces we used a Kistler Dynamometer 9257B. This dynamometer uses a piezoelectric crystal to measure forces on all three axes. The dynamometer produces an output in millivolts. To convert the millivolts to Newtons, the dynamometer has a sensitivity conversion on 10mV/N in the X and Y directions and 5mV/N in the Z direction.

Technical Data

Dynamometer Type 9257BA

Range 1	F_x, F_y	kN	–0,5 … 0,5
	F_z	kN	–1 … 1
Range 2	F_x, F_y	kN	–1 … 1
	F_z	kN	–2 … 2
Range 3	F_x, F_y	kN	–2 … 2
	F_z	kN	–5 … 5
Range 4	F_x, F_y	kN	–5 … 5 [1]
F_z for F_x and F_y ≤0,5 F_z	F_z	kN	–5 … 10 [2]
Overload	F_x, F_y, F_z	kN	–7,5/7,5
F_z for F_x and F_y ≤0,5 F_z	F_z	kN	–7,5/15
Threshold		N	<0,01
Sensitivity	F_x, F_y	mV/N	10,0
Range 1	F_z	mV/N	5,00
Linearity, all ranges		% FSO	≤±1
Hysteresis, all ranges		% FSO	≤0,5
Cross talk		%	≤±3
Rigidity	c_x, c_y	kN/µm	>1
	c_z	kN/µm	>2
Natural frequency	f_n (x,y)	kHz	≈2,0
(mounted on flanges)	f_n (z)	kHz	≈3,5
Operating temperature range		°C	0 … 60
Drift (charge amplifier)	F_x, F_y	N/s	≤±0,005
at 25 °C	F_z	N/s	≤±0,01
Ground isolation		MΩ	>100
Connecting cable (integral)	l	m	5
Degree of protection			IP 67
Weight		kg	7,4

[1] Application of force inside and max. 25 mm above top plate area.
[2] Range for turning, application of force at point A.

Figure 36: Kistler Dynamometer Technical Data Sheet (Kistler, 2017)

2.2.3 Procedure

To measure the slicing forces in the x, y, and z directions we designed a system using a Kistler dynamometer, a Kistler amplifier, a National Instruments Data Acquisition Box, and the National Instruments LabVIEW software. For more information on the procedure, please refer to Appendix B.

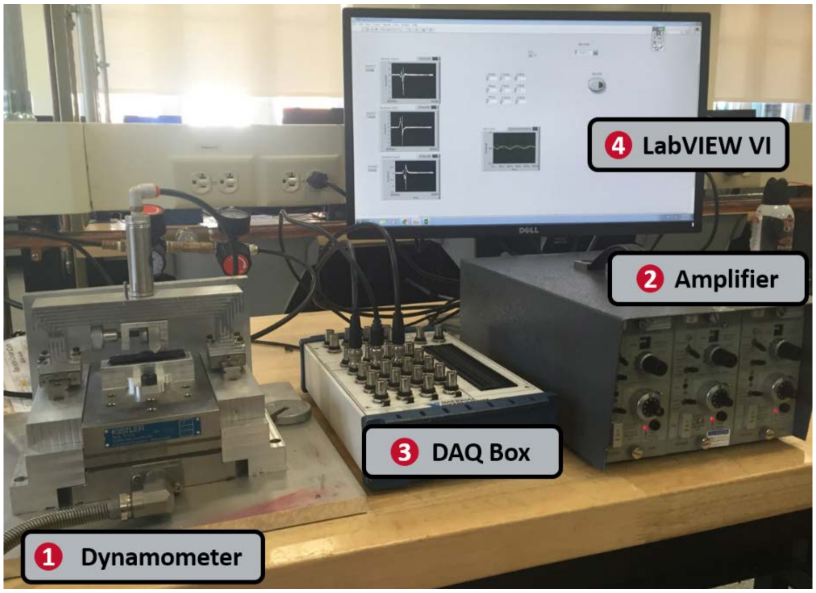

*Figure 37: Test Setup in Experimentation Lab (*LabVIEW*)*

2.3 Surface Metrology

2.3.1 Surface Measurements

To measure both the aluminum edges and the paraffin wax samples we used an Olympus Lext OLS4100 confocal microscope. The 50x low standoff zoom was used the measure the aluminum edges before slicing. The 20x zoom was used to measure the paraffin wax after slicing. For more information about how we prepared and measured the materials please refer to Appendix A and Appendix C.

2.3.2 Use of MountainsMap

MountainsMap is a program developed by DigitalSurf that can be used to interpret and analyze measurements taken by the Olympus microscope. MountainsMap was used to filter out topographic layers, analyze the topographic layer, find parameter values, and calculate curvature. For more information about the use of MountainsMap please refer to Appendix A.

2.3.3 Use of SFrax

SFrax was used primarily for area-scale analyses and complexity analyses. We also used the SFrax software to perform regression analyses for both curvature versus relative area and curvature versus complexity.

3. Results

3.1 Force Component Measurements

After experimentally testing the blade edges in our testing device, we were able to obtain force component measurements from the dynamometer through our LabVIEW script, which we then used to export the data to Excel for further analysis. Using Excel, we developed the following graphs of force components F_x, F_y, and F_z, over time. The gradual declination in between the force and the cutting formation and the reaction force is known as stick-slip. The stick-slip occurred when the edge was slicing through the substrate, became "stuck" at a point during the slicing motion, and the increased pressure in the air cylinders acting on the sliding rail caused the edge to overcome the obstruction. The figure below shows the force vs. time graph with an example of the stick-slip occurrence.

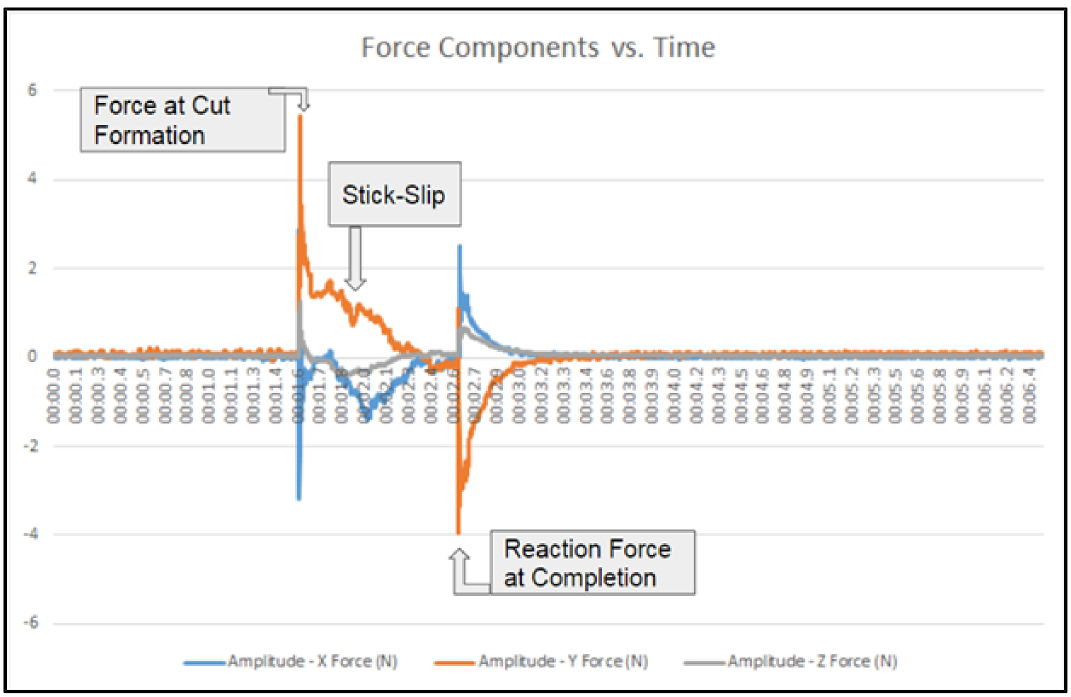

*Figure 38: Example of Force vs. Time Graph with Stick Slip (*Microsoft Excel*)*

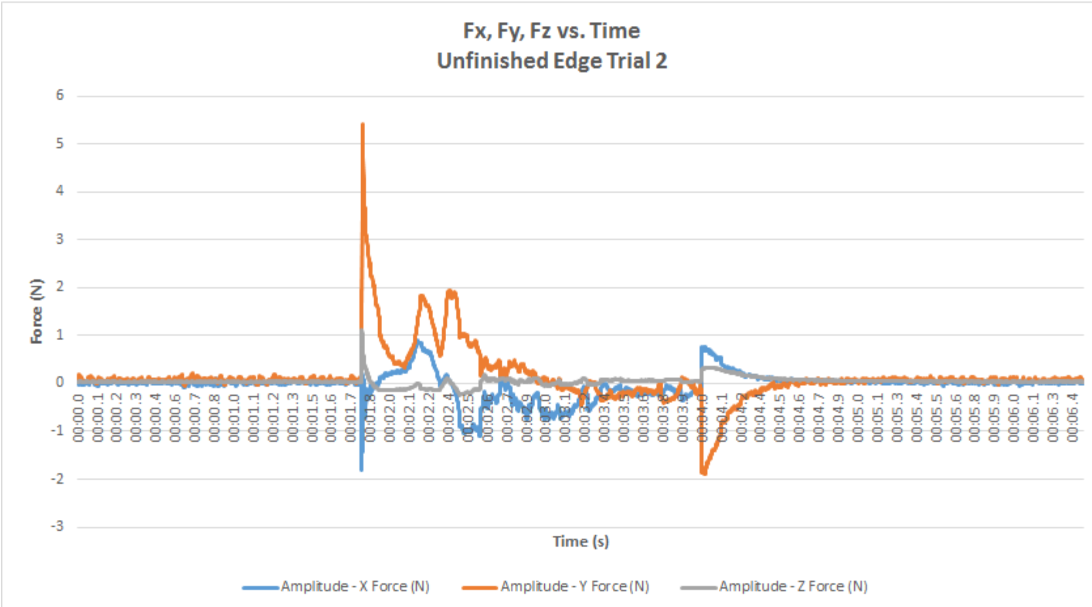

*Figure 39: Force vs. Time- Unfinished Edge (*Microsoft Excel*)*

As can be seen in the above measurements, the tangential force at cut formation, F_y, is approximately 5.41N, and the normal force at cut formation, F_z, is approximately 1.13N. These measurements correlate with our findings in Section 1.3, where edges that are generally less sharp (larger tip radius) require greater force for cut formation in slicing through a substrate. The figure below graphically represents the data acquired from the same procedure, but with an edge polished with a 1500 grit polishing kit. The cut formation occurs at approximately t = 1.7s, with a tangential force of 3.73N and a normal force of 0.36N. With the sharper and less rough edge (smaller tip radius and relative area), the normal and tangential forces at cut formation were reduced.

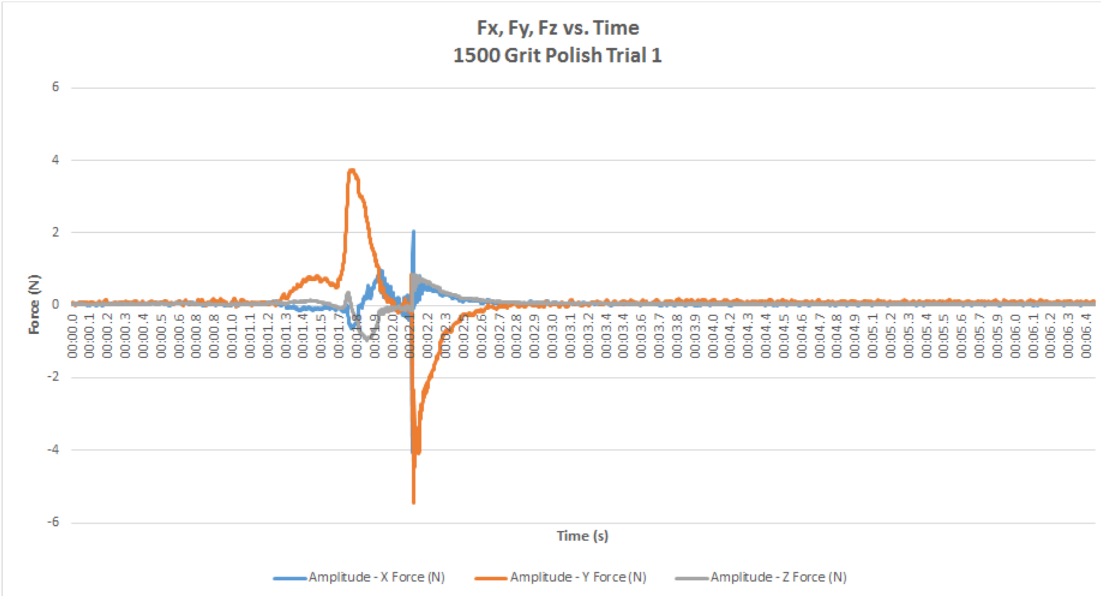

*Figure 40: Force vs. Time- 1500 Grit Polish Edge (*Microsoft Excel*)*

The tangential force of the edge in this instance increased and decreased from approximately t=1.3s to t=1.65s, forming a curve, instead of a rapid spike in force. When the edge became unstuck, the tangential force greatly increased to the force at cut formation. The stick-slip could be attributed to the air flow in the cylinders, as well as the interaction between material properties of the paraffin wax and aluminum edges. Another trend in the above graphs that we observed was the instantaneous decrease in the tangential force when the edge comes to a stop at the end of the trial. This reaction force was read by the dynamometer, and it can be observed at t=2.1s in the above figure.

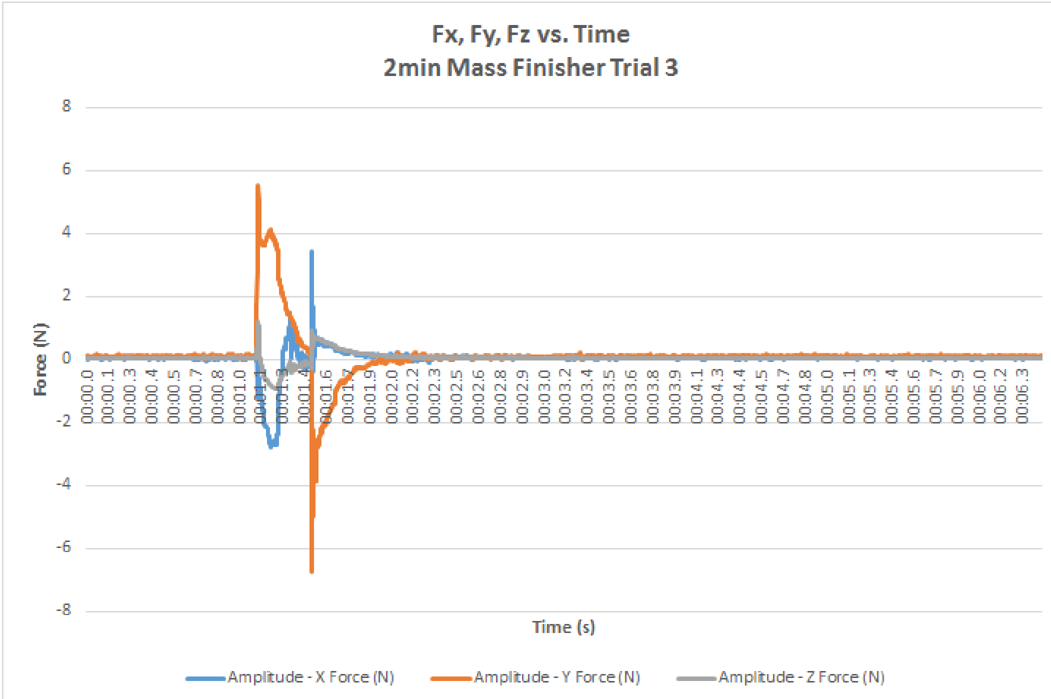

*Figure 41: Force vs. Time- 2 Minute Mass Finished Edge (*Microsoft Excel*)*

The 2 minute mass finished trial shown in the figure above shows an initial force at the cut formation of approximately 5.29N at t=1.1s. There is a large amount of stick-slip observed from t=1.2s to t=1.3s. The reaction force is larger than the initial force at the cut formation because the stick-slip could account for some of the absorbed force.

The 8 minute mass finished trial, in the figure below, has an initial force at the cutting formation of 1.76N at t=1.9s. There is almost no stick-slip and the reaction force is 1.75N. This accurately shows that the energy lost while slicing can mostly be attributed to the stick-slip. The force needed to slice is also less than most of the other trials, which can likely be attributed to a dull edge needing less force to slice through a material.

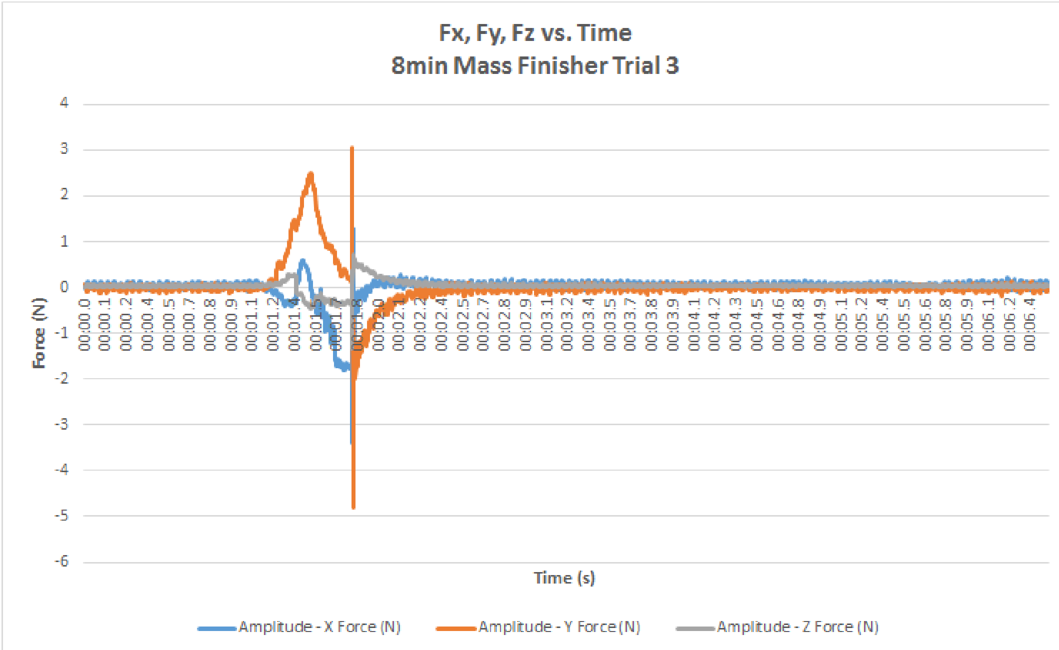

*Figure 42: Force vs. Time: 8 Minute Mass Finished Edge (*Microsoft Excel*)*

3.2 Curvature Measurements

The curvature was calculated using Heron's formula in the CurvSoft program. Our team took the profile of the edge from MountainsMap, and exported the file to CurvSoft. This program gave us the curvature of the edge at various scales. This information was then exported back to MountainsMap, where an advanced contour analysis was completed at the most optimal scale. We show the curvature analysis for the 3000 grit polished edge in this section of the report. The curvature for this edge is 13.0µm at the 150µm scale. The curvature analyses for the remaining edges can be seen in Appendix A.

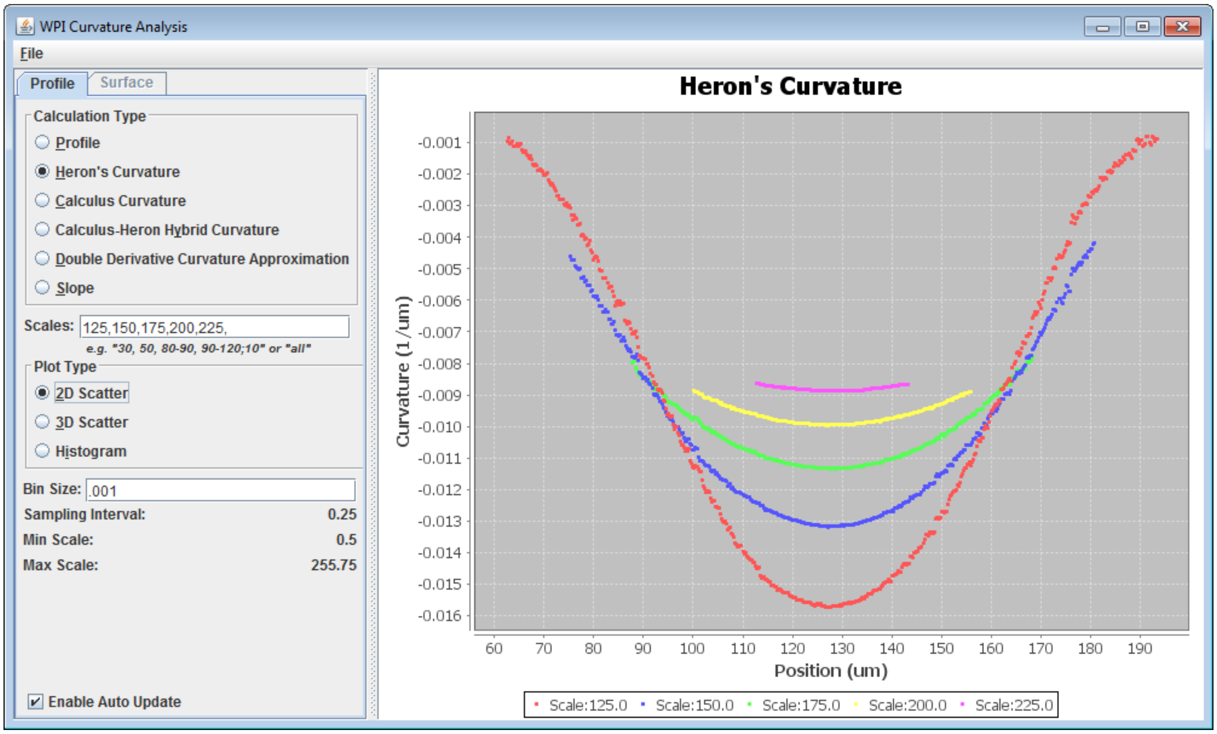

Figure 43: CurvSoft- Heron's Curvature of Edge at Various Scales (Curvsoft)

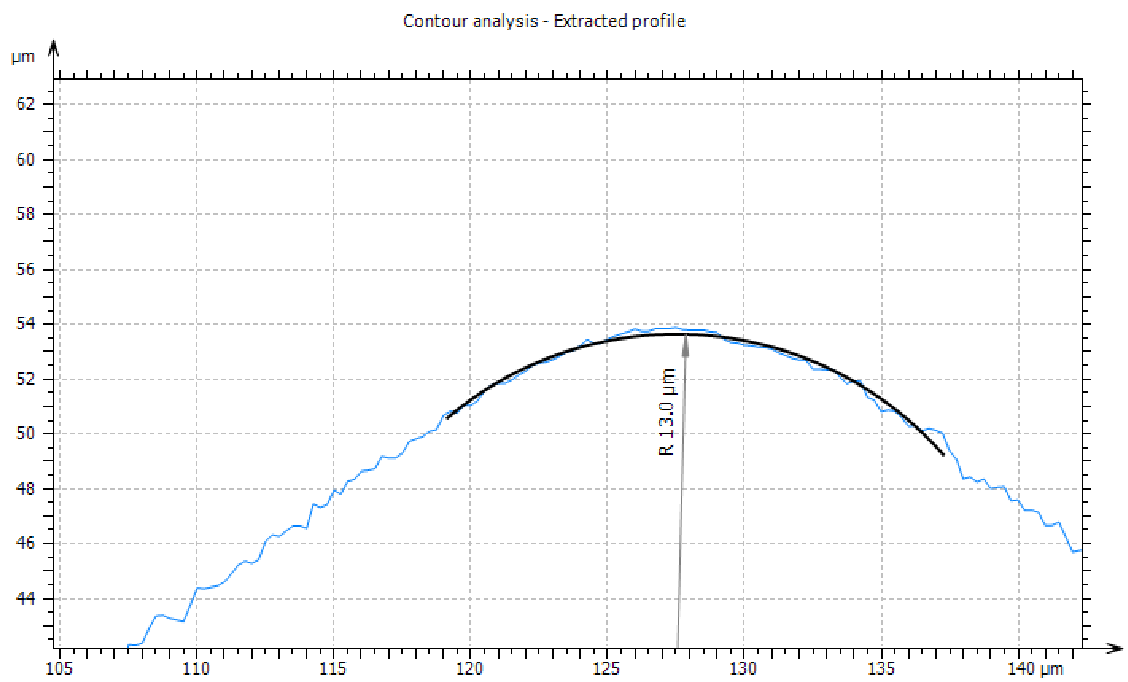

Figure 44: Curvature Analysis- 3000 Grit Polished Edge at Scale of 150µm (MountainsMap)

3.3 Surface Measurements

After slicing through the different wax samples with aluminum edges, we were able to examine the paraffin wax samples under the Olympus microscope. We used the unfinished edge, along with polished edges using sandpaper grits of 1200, 1500, 2000, and 3000. We also used edges that were put through the mass finisher for 2 minutes, 4 minutes, and 8 minutes. We tested three wax samples with each edge. Once under the microscope, we used the 20x magnification lens to examine the valley of the wax samples. We were able to use the 20x lens because it had a standoff of 1000 micrometers before reaching the sample. The maximum depth of our wax samples after slicing was only about 900 micrometers, allowing us to safely measure the wax without crashing the lens. Examples of the wax sample after testing for the unfinished, 1200 grit polished, and 2 minute mass finished edges are shown below. The remaining trials for each wax sample can be found in Appendix D, along with outlier information.

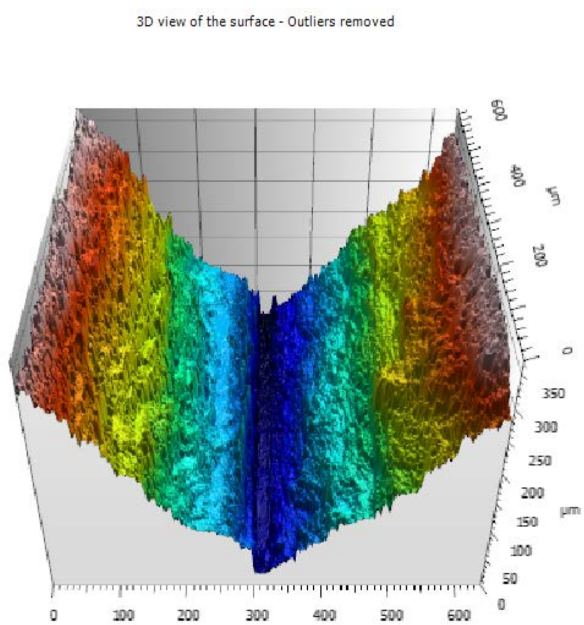

Figure 45: Unfinished Edge Trial 1 Wax (MountainsMap)

The unfinished edge wax sample can be seen in the figure above. This trial resulted in a rough finish on the wax, from the non-polished edge. The shape of the wax is a result of the large burr that is present on the unfinished edge.

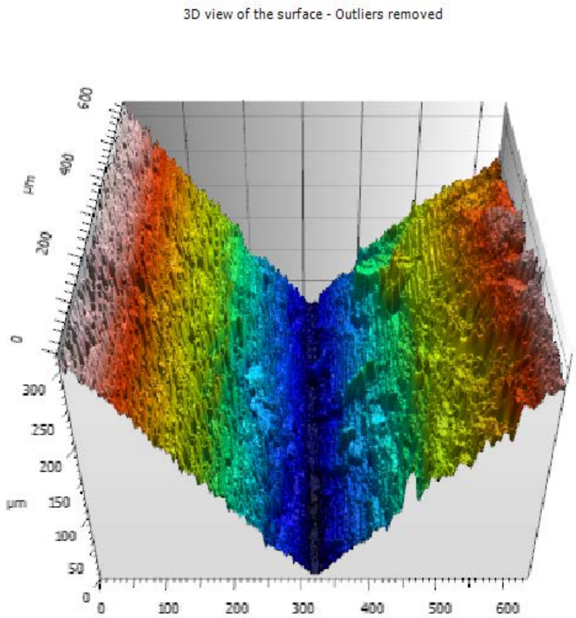

Figure 46: 1200 Grit Polished Edge Trial 1 Wax (MountainsMap)

The 1200 grit polished edge produced the above wax sample. The polished edge created a smoother slice through the wax and has a fine point in the valley of the cut. It was seen that as the sandpaper grits increased, the point in the valley became more defined.

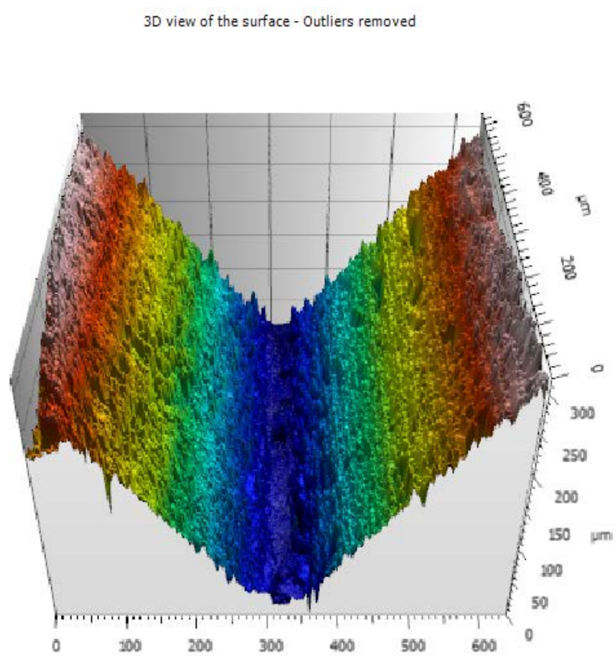

Figure 47: 2 Minute Mass Finished Edge Trial 3 Wax (MountainsMap)

The 2 minute mass finished edge, in the figure above, produced a round valley, as opposed to the pointed valley resulting from the polished edges. The roughness along the sidewalls of the cut was also greater than that of the polished edges, which was predictable based on the finish created by the mass finisher.

3.4 Correlation Results

3.4.1 Relative Area vs. Scale Analysis

To perform multi-scale geometric analysis, our team used SFrax. We performed an area-scale analysis for each edge that we tested. The results can be seen in the figure below. There is a clear difference between the unfinished edge and the polished and mass finished edges. All of the polished edges are almost indistinguishable at all scales. There is a minor separation in the mass finished edges due to the edges increasing in roughness as the time in the mass finisher increases.

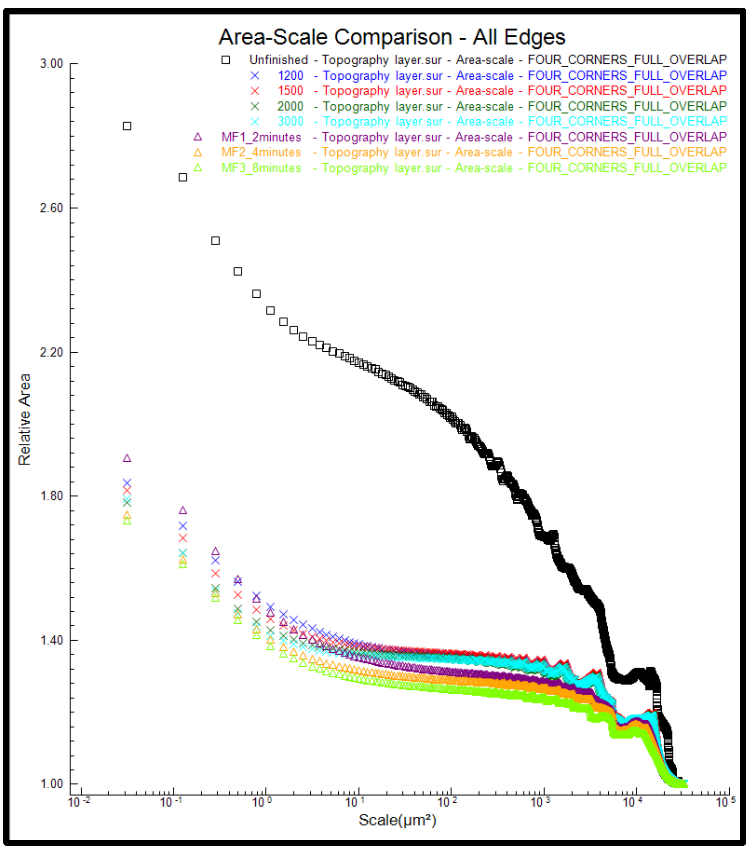

Figure 48: Relative Area vs. Scale Analysis all Edges (SFrax)

3.4.2 Relative Area Regression Analysis

After doing a regression analysis for curvature vs. relative area, we noticed at the finer scales there is a 0% correlation. At the larger scales, 10^4µm to 10^5µm there is a 35% correlation, however, with the larger scales there is usually a great deal of noise, which could contribute to that spike. Based on this information, we can state there does not appear to be a significant correlation between the two at any scale. This might be due to the curvature being such a small area compared to the relative area of the edge.

.

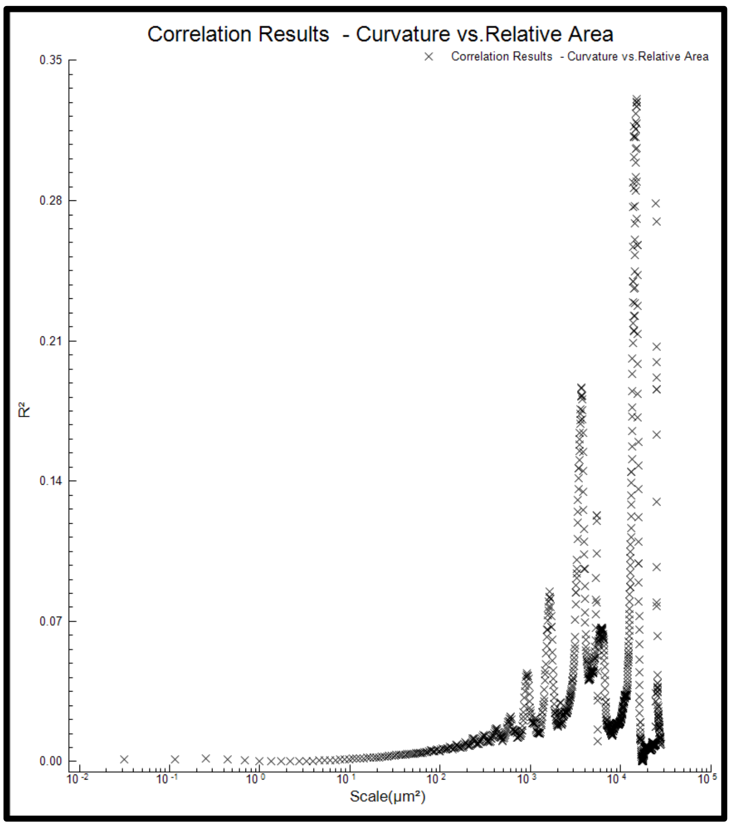

Figure 49: Curvature vs. Relative Area Regression Analysis (SFrax)

3.4.3 Complexity vs. Scale Analysis

We performed a complexity analysis for each edge that we tested. The results can be seen in the figure below. There is a clear difference between the unfinished edge and the polished and mass finished edges. Again, all of the polished edges are almost indistinguishable at all scales. There is a minor separation in the mass finished edges due to the geometry being altered as the time in the mass finisher increases.

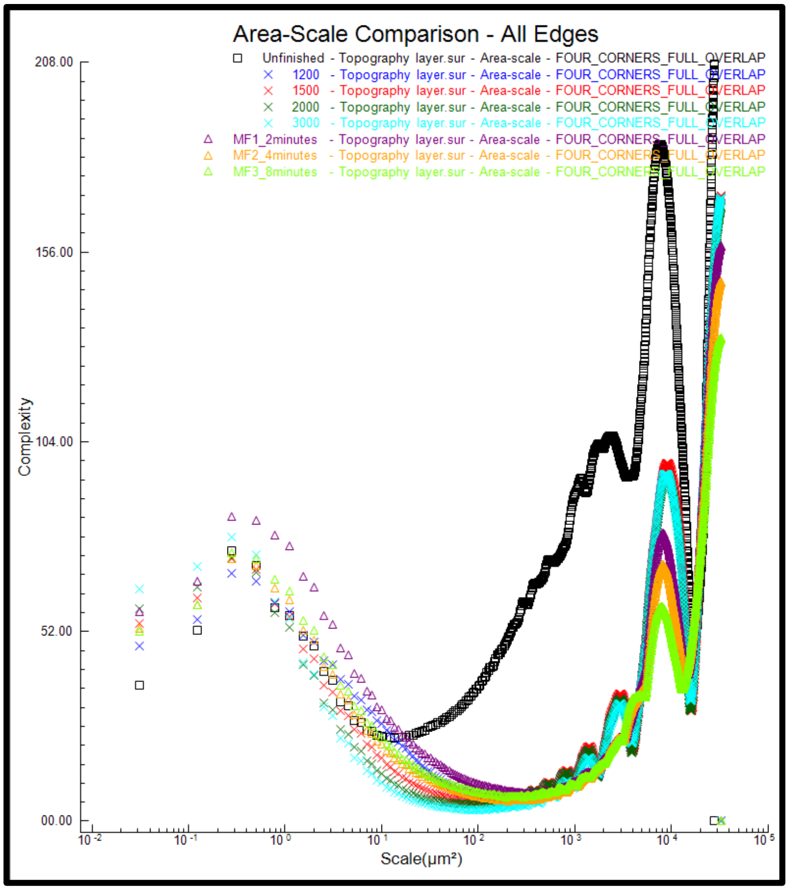

*Figure 50: Complexity vs. Scale Analysis all Edges (*SFrax*)*

3.4.4 Complexity Regression Analysis

After completing a regression analysis for complexity, at low scales there does not appear to be a strong correlation between curvature and the complexity of the edge. At higher scales, 10^4µm to 10^5µm, there appears to be a strong correlation, 99%. However, much of this is most likely due to noise at the higher scales.

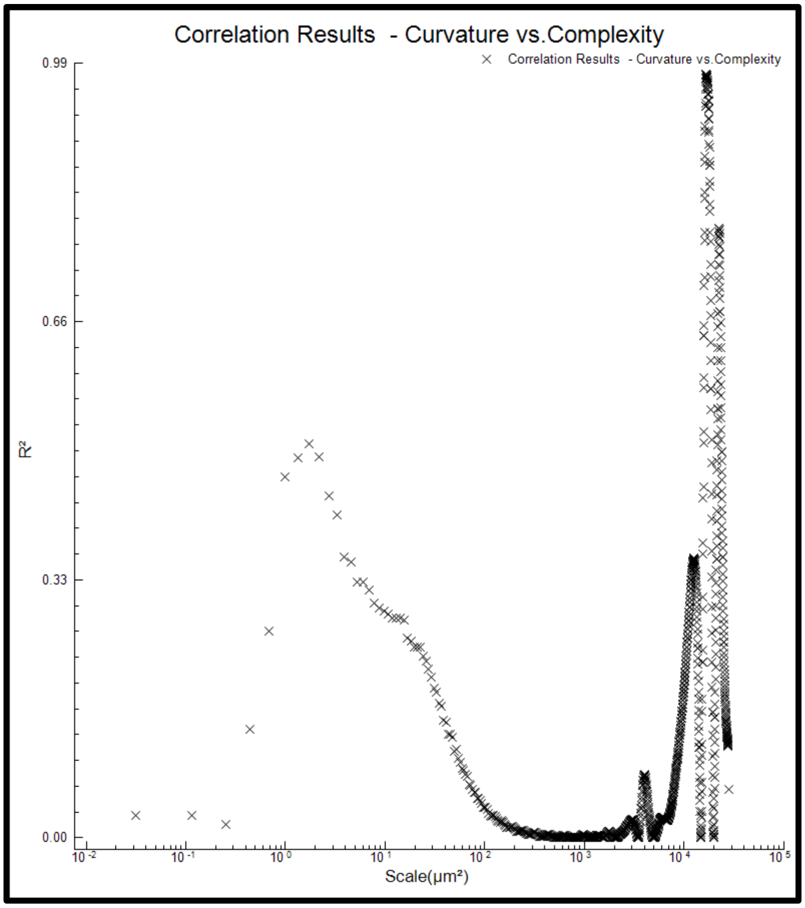

*Figure 51: Curvature vs. Complexity Regression Analysis (*SFrax*)*

4. Discussion

4.1 Force Testing

The testing apparatus used in our experiment was a modified version of a testing apparatus used by a previous MQP team at WPI. We needed to adapt their scraping device to account for our slicing testing. We also needed to add a fixture to hold the material during the testing. A piece of the apparatus that was pre-existing was the pneumatic portion. This comprised of the air cylinders with hoses running to dial knobs with the PSI gauges on them, which were fed by the forced air system in Higgins Engineering Experimentation Lab. A problem we believe to have had was an inconsistent amount of air, or force, in the experiment. The dials needed to be turned, which would then slowly open the flow of air to the cylinders. This made the experiment difficult to replicate for each trial, particularly with the horizontal air cylinder. If there was a modification made to the air system, our team believes the results from the trials would become more repeatable and consistent. If there was some sort of solenoid added to the system after the dials, we believe the results would change. This way, the user could set the correct pressure with the dials and then with a press of a button, the solenoid would open and exactly the amount of air would flow to the cylinders almost instantaneously. This would help reduce the amount of stick-slip in the experiment, which in turn, should give more accurate results for instantaneous force at cut formation.

4.2 Limitations

4.2.1 Razor Blades and Precision Slicing Blades

The microscope in combination with MountainsMap software could not accurately measure curvature for razor blades and precision slicing blades. This set our team back because our initial plan was to use these blades for testing. Please refer to Appendix G for more information.

4.2.2 Depth of Cut

After initial trials of slicing 90 degree edges through paraffin wax, we wanted to measure the depth of the slices being made. The lens on the Olympus microscope to measure this would be the 5x lens because it can measure the entire field necessary. The 5x lens is not very accurate and since it has such a high standoff it produces a considerable amount of noise. We then only used the 20x lens to measure the wax after slicing, which had a smaller field of view, as can be seen in the figure below. Since our measurements with the 5x lens were not deemed to be accurate, we decided not to pursue using depth of cut in our analyses.

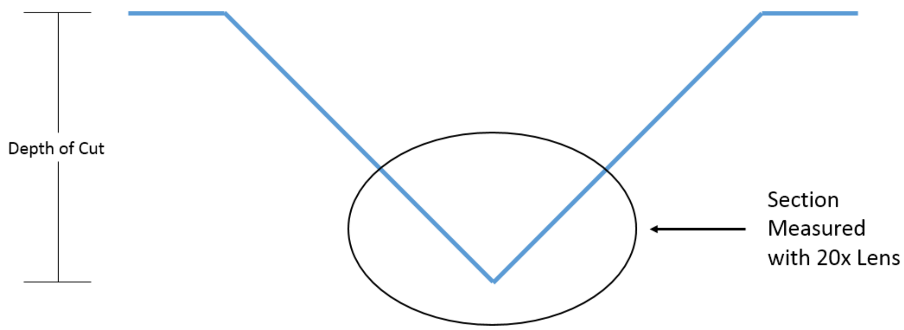

Figure 52: Depth of Cut Limitation Diagram

4.2.3 Procedure

Being that there has not been much previous research done in the field of slicing, this project proved to be quite complex. There is little in the literature to refer to for procedures and guidelines for testing the force of slicing and measuring the curvature of the edges and performance of the cut. Our team realized this and attempted to create some sort of baseline testing device and curvature analysis procedure based on techniques used by past MQP groups and the staff of the WPI Surface Metrology Lab. We understand that this was a starting point and acknowledge that there most likely will need to be changes in the procedure to get more accurate testing results and then curvature analyses.

4.2.4 Future Analyses

Our analyses were limited by the amount of time we had to complete the project. We only compared 2-D data sets. In future research, the comparison should be made for relative area versus curvature scale data where single value analyses could be scaled up to multi value analyses. This kind of comparison would lead to more complex data analysis, which would hopefully lead to more correlations in this research. For repeatability of this experimental process, the recommendations presented in Section 4.1 regarding the force testing procedures should be taken into consideration. Also, the procedural flaws in this pioneering experimental procedure could have contributed to the lack of definitive correlations between curvature, complexity, and relative area.

5. Conclusions

1. We believe the Stick-Slip hypothesis results in a great loss of initial slicing force.
2. A polishing technique where the edge is polished parallel to the tip provides a cleaner curvature at the edge. This results in a simpler geometric shaped slice with the burr removed.
3. There appears to be a strong correlation between curvature and complexity at higher scales, 10^4µm to 10^5µm, however, this could be due to noise in our measurements.
4. There is not a strong correlation between curvature and relative area at any scale.
5. A more accurate means to measure depth of cut needs to be identified, in order to calculate regression analyses between depth of cut, force, relative area, and complexity.
6. Future work on this subject matter should be done to enhance repeatability and further investigate correlations.

6. References

Curvsoft. (2017). Worcester, MA.

ESPRIT CAM. (2017). Camarillo, CA.

Gleason, M.A., Kordell, S.,. Lemoine, A., Brown, C.A. (2013). Profile Curvatures by Heron's Formula as a Function of Scale and Position on an Edge Rounded by Mass Finishing, *14th International Conference on Metrology and Properties of Engineering Surfaces*, Taipei, Taiwan , paper TS4-01, 0022.

Kistler. (2017). *Data Sheet, 3-Component Dynamometer Fx, Fy, Fz, Type 9257BA.*

Korecki, T., Pałka, D., & Wąs, J. (2016). Adaptation of Social Force Model for simulation of downhill skiing. *Journal of Computational Science, 16*, 29-42.

LabVIEW. (2017). Austin, TX.

Leonov, S. and Badiaev, V. (2016). Forensic medical characteristics of stab wounds caused by objects differing in the blade sharpness. *Sudebno-meditsinskaia Ekspertiza*, 52(2), pp.16-18.

Microsoft Excel. (2017). Redmond, WA.

McCarthy, C., Annaidh, A. and Gilchrist, M. (2010). On the sharpness of straight edge blades in cutting soft solids: Part II – Analysis of blade geometry. *Engineering Fracture Mechanics*, 77(3), pp.437-451.

McCarthy, C., Hussey, M. and Gilchrist, M. (2007). On the sharpness of straight edge blades in cutting soft solids: Part I – indentation experiments. *Engineering Fracture Mechanics*, 74(14), pp.2205-2224.

McGorry, R., Dowd, P. and Dempsey, P. (2003). Cutting moments and grip forces in meat cutting operations and the effect of knife sharpness. *Applied Ergonomics*, 34(4), pp.375-382.

Moreno, M., Brown, C. and Bouchon, P. (2010). Effect of food surface roughness on oil uptake by deep-fat fried products. *Journal of Food Engineering*, 101(2), pp.179-186.

MountainsMap. (2017). Besançon, France.

Reyssat, E., Tallinen, T., Le Merrer, M. and Mahadevan, L. (2012). Slicing Softly with Shear. *Physical Review Letters*, 109(24).

Schuldt, S., Arnold, G., Kowalewski, J., Schneider, Y. and Rohm, H. (2016). Analysis of the sharpness of blades for food cutting. *Journal of Food Engineering*, 188, pp.13-20.

SFrax. (2017). Worcester, MA.

SolidWorks. (2017). Waltham, MA.

Tsai, P., Lin, Y., Li, J., Jian, S., Jang, J., Li, C., Chu, J. and Huang, J. (2012). Sharpness improvement of surgical blade by means of ZrCuAlAgSi metallic glass and metallic glass thin film coating. *Intermetallics*, 31, pp.127-131.

Viestenz, A., Langenbucher, A., Hofmann-Rummelt, C., Modis, L., Viestenz, A. and Seitz, B. (2003). Evaluation of corneal flap dimensions and cut quality using the SKBM automated microkeratome. *Journal of Cataract & Refractive Surgery*, 29(4), pp.825-831.

Wilson, A. (2016). *Ski with tunnel and enhanced edges*. U.S. Patent no. 7,073,810.

Appendix

Appendix A: Curvature Analysis

The curvature analyses for the edges not found in Section 3.2 can be found below. These figures are the advanced contour analysis profiles imported into MountainsMap from CurvSoft.

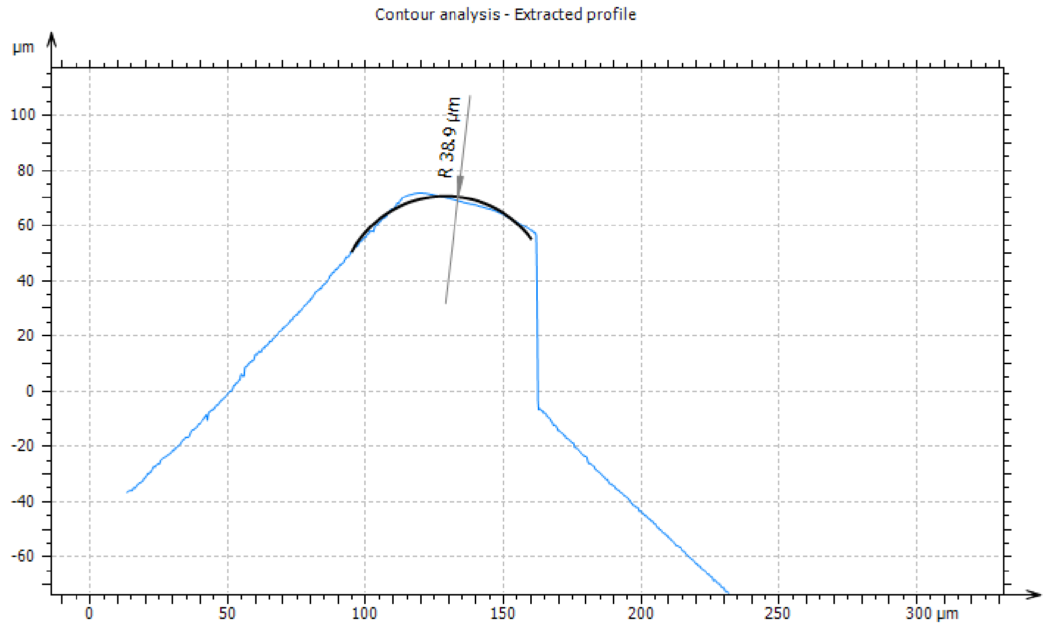

Figure 53: Curvature Analysis- Unfinished Edge (MountainsMap)

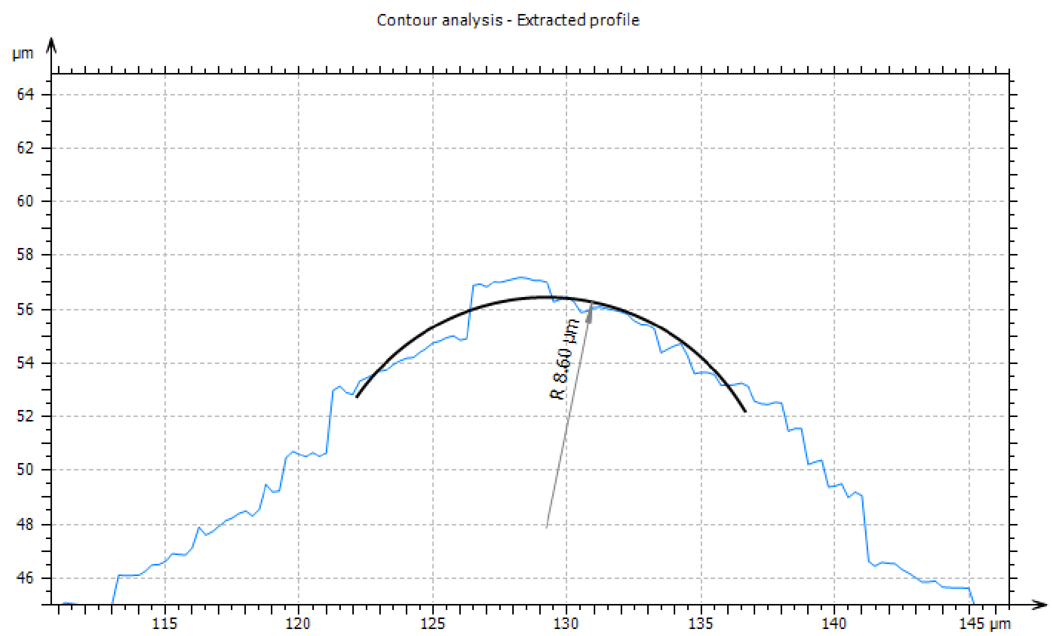

Figure 54: Curvature Analysis- 1200 Grit Polished Edge (MountainsMap)

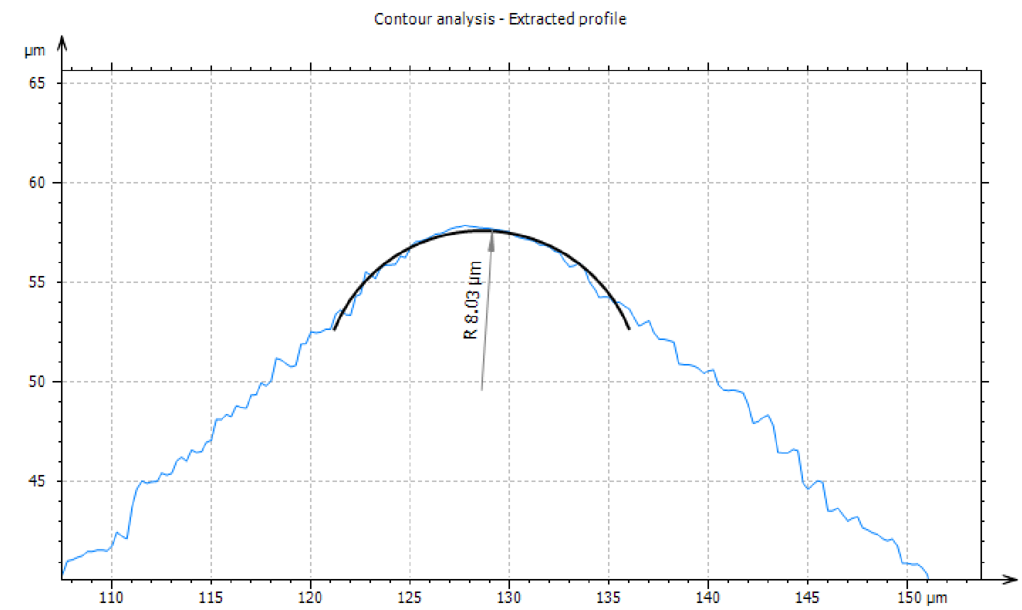

Figure 55: Curvature Analysis- 1500 Grit Polished Edge (MountainsMap)

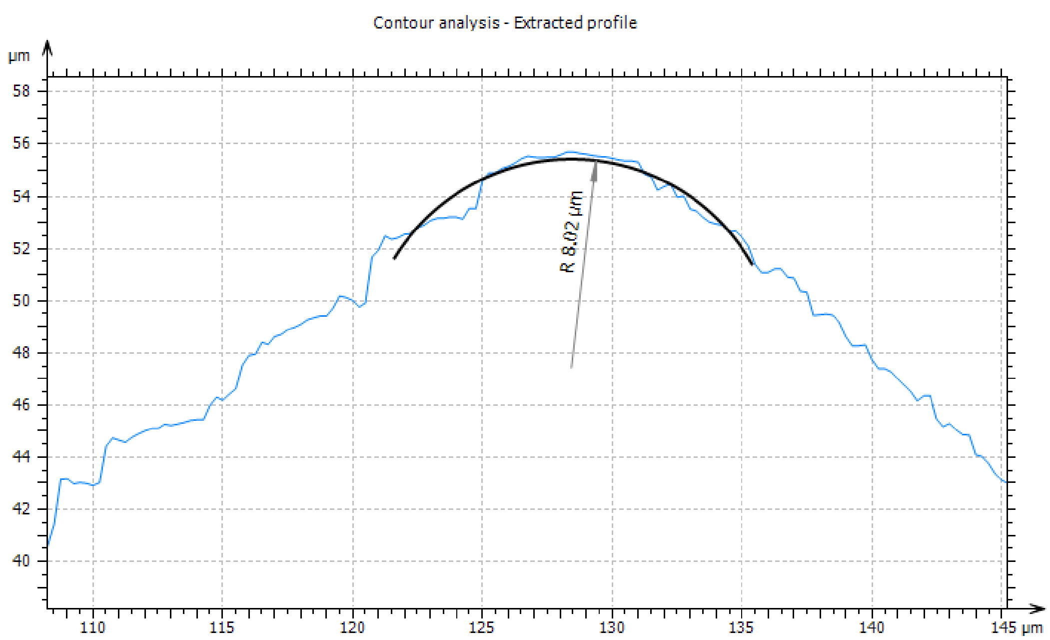

Figure 56: Curvature Analysis- 2000 Grit Polished Edge (MountainsMap)

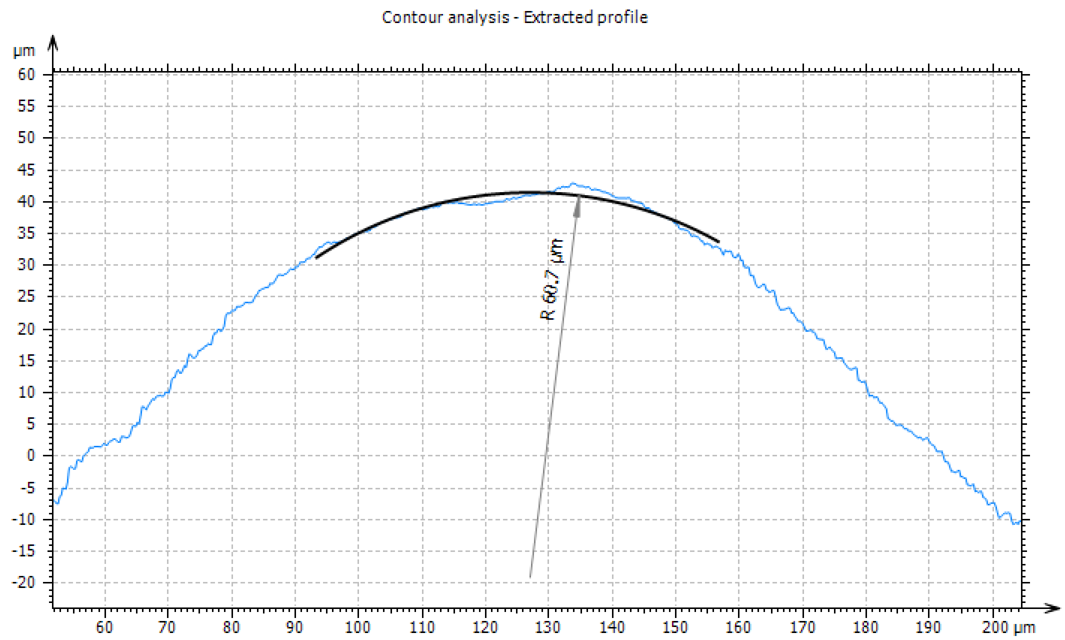

Figure 57: Curvature Analysis- 2 Minute Mass Finished Edge (MountainsMap)

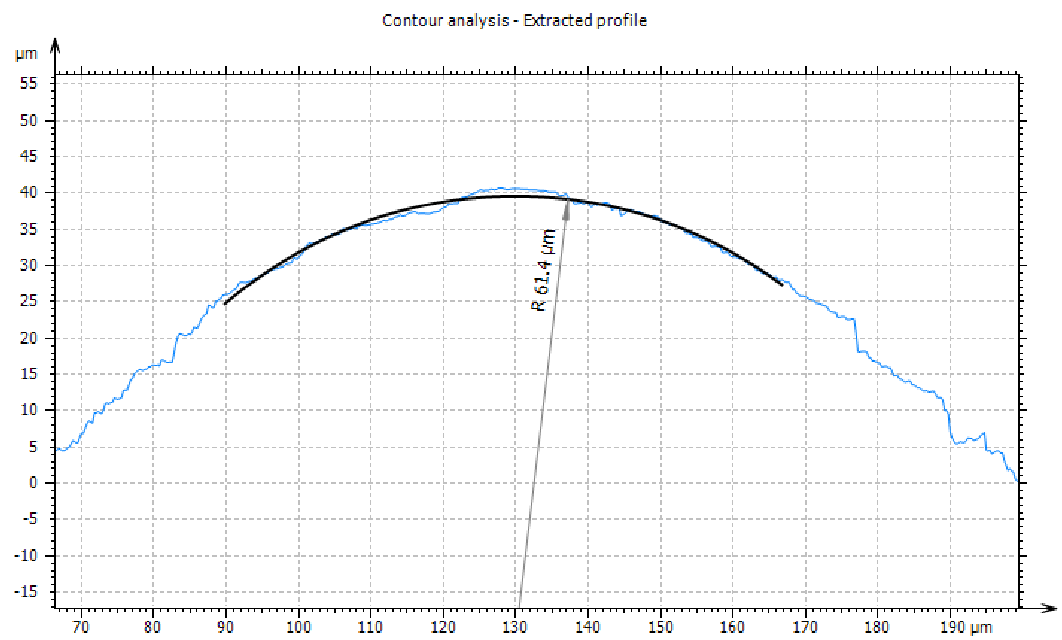

Figure 58: Curvature Analysis- 4 Minute Mass Finished Edge (MountainsMap)

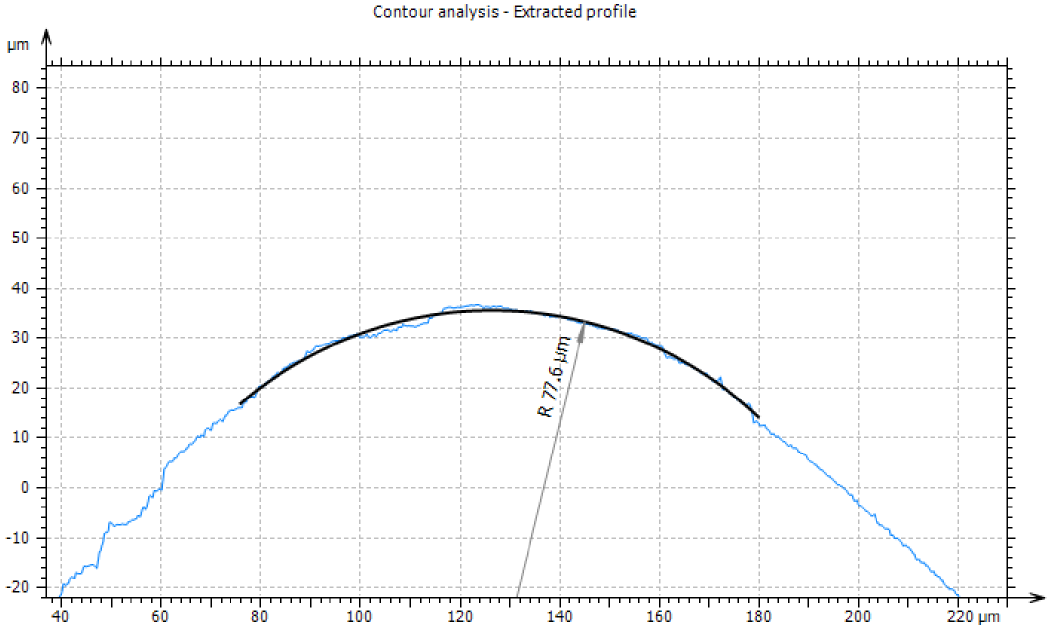

Figure 59: Curvature Analysis- 8 Minute Mass Finished Edge (MountainsMap)

Appendix B: Apparatus

Below are images of the 3D CAD models and the CAM simulation results of the parts our team designed and manufactured for the testing apparatus. All CAD work was done using Solidworks and all CAM work was done using Esprit. Most of the machining was done on a Haas Minimill CNC machine, while some (tapping) was done by hand.

Edge Fixture

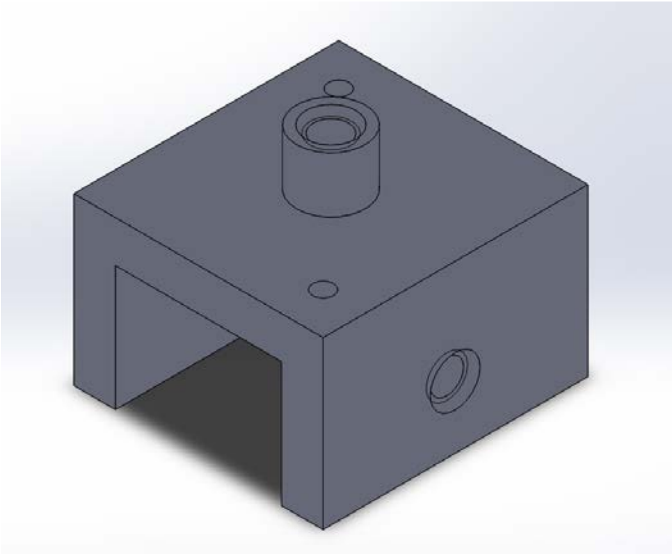

Figure 60: Edge Fixture Solidworks 3D Model (SolidWorks)

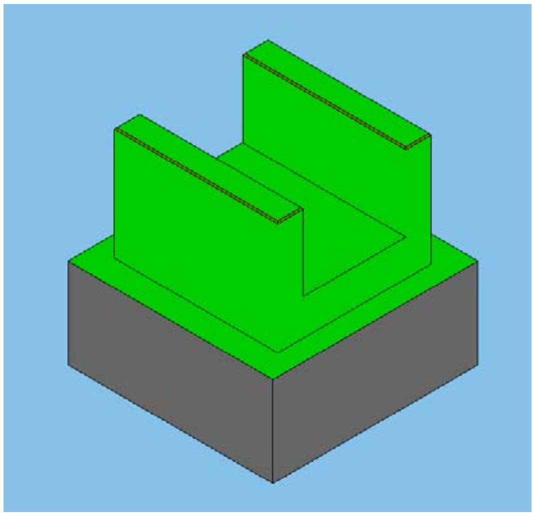

Figure 61: Edge Fixture CAM OP1 (ESPRIT)

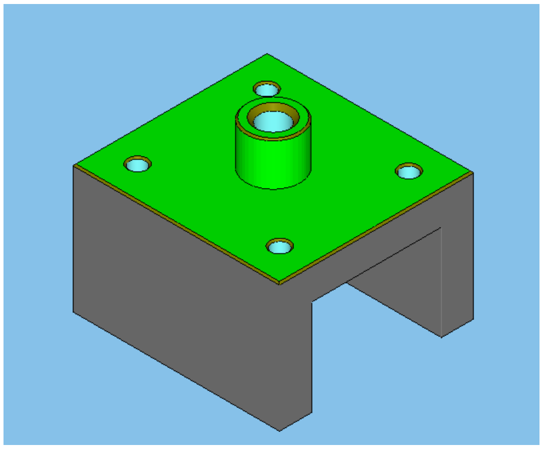

Figure 62: Edge Fixture CAM OP2 (ESPRIT)

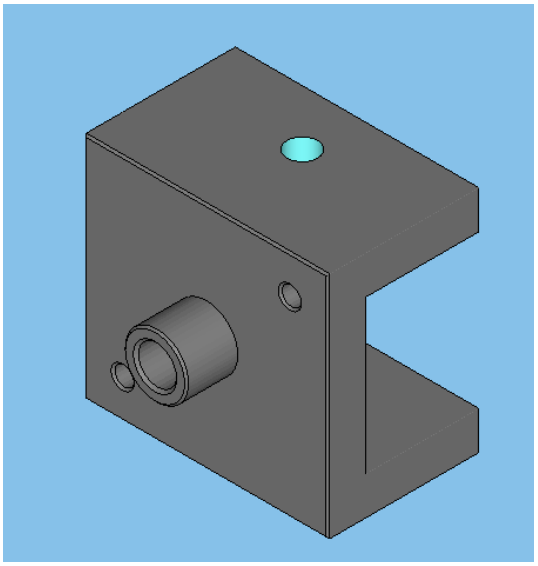

Figure 63: Edge Fixture CAM OP3 (ESPRIT)

Material Fixture

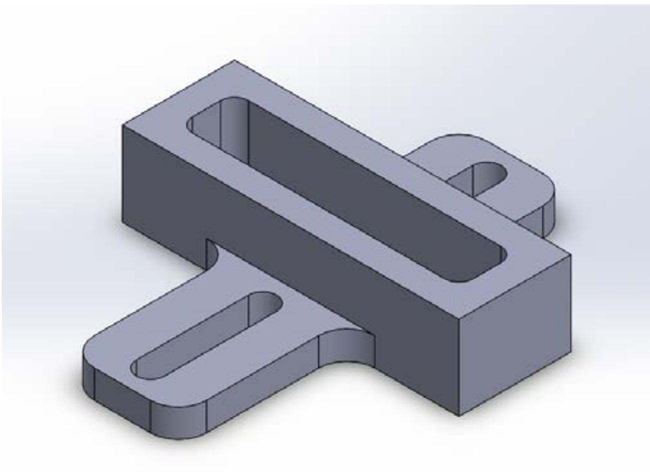

Figure 64: Material Fixture Solidworks Model (SolidWorks)

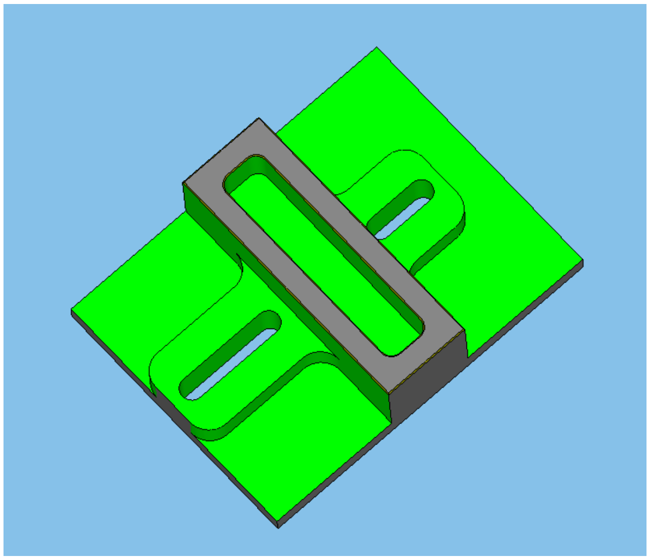

Figure 65: Material Fixture CAM OP1 (ESPRIT)

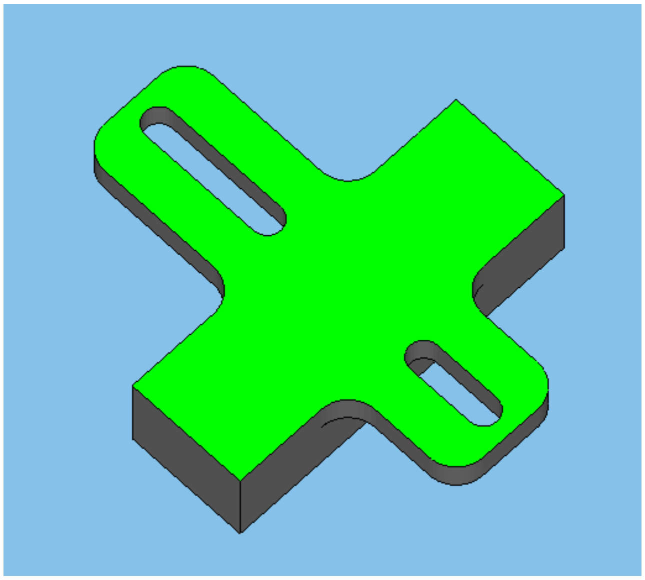

Figure 66: Material Fixture CAM OP2 (ESPRIT)

Linear Bearing Spacer

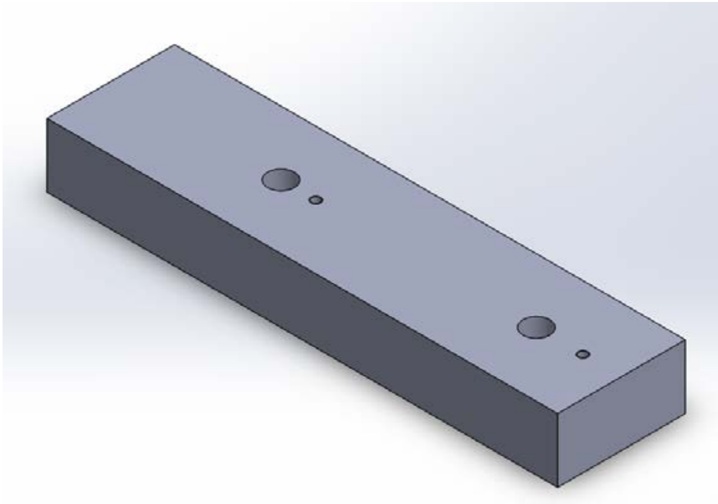

Figure 67: Linear Bearing Spacer Solidworks Model (SolidWorks)

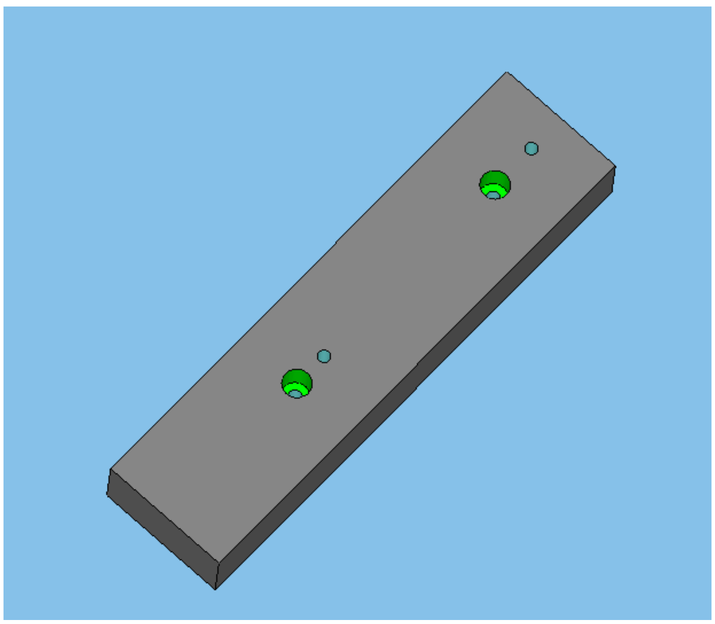

Figure 68: Linear Bearing Spacer CAM (SolidWorks)

Back Plate

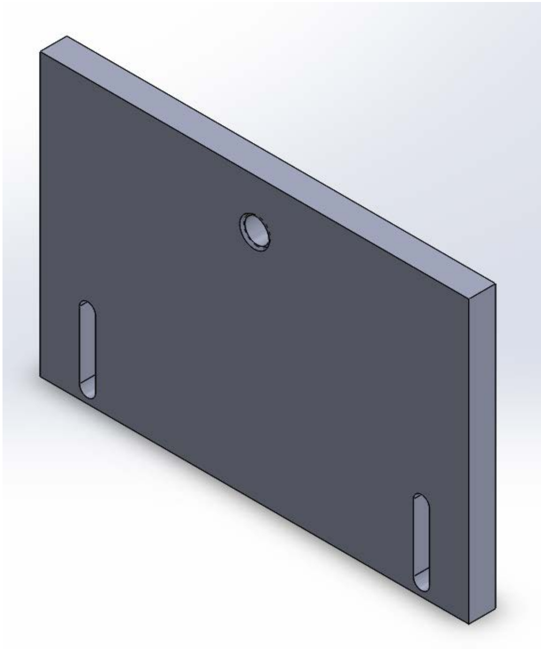

Figure 69: Back Plate Solidworks Model (SolidWorks)

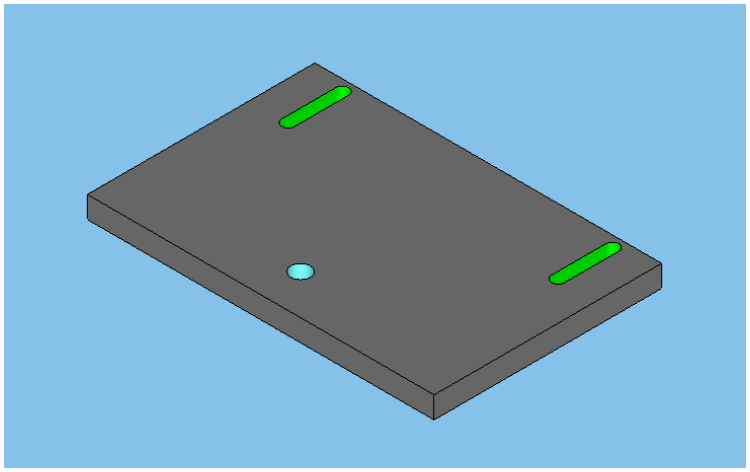

Figure 70: Back Plate CAM (ESPRIT)

Sliding Rail

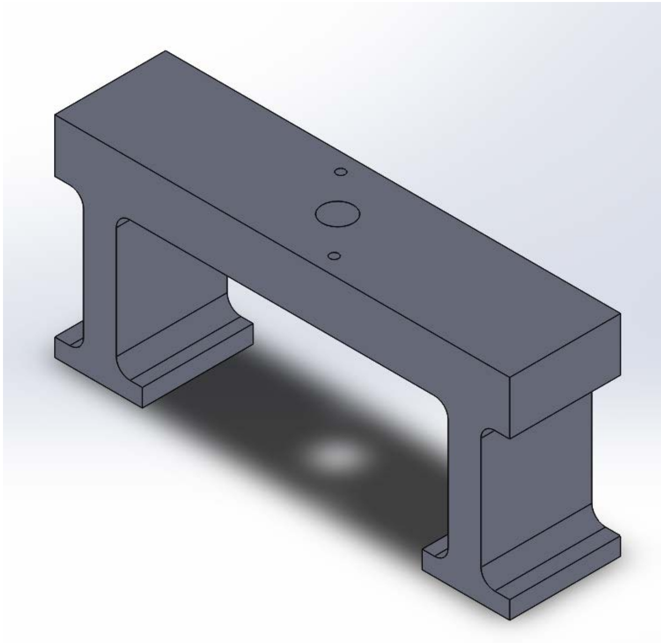

Figure 71: Sliding Rail Solidworks Model (SolidWorks)

Appendix C: Edges

In the first machining and polishing trials, we looked at the 90 degree edges under the Olympus microscope after polishing the edges with 1200, 1500, and 2000 grit sandpaper. We also looked at a machine finished edge without any polishing as a baseline for our results. This also helped us figure out where our error was coming from.

Unfinished - As seen in the images below, there is a curve on one side of the edge, and the opposite side has more of a linear slope. This has to be due to a machining issue since no polishing has been done on this edge.

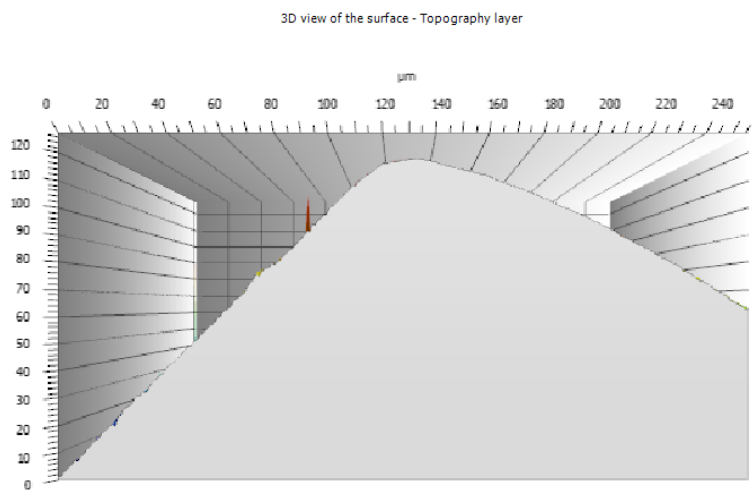

Figure 72: Trial 1- Unfinished Edge 2D View (MountainsMap)

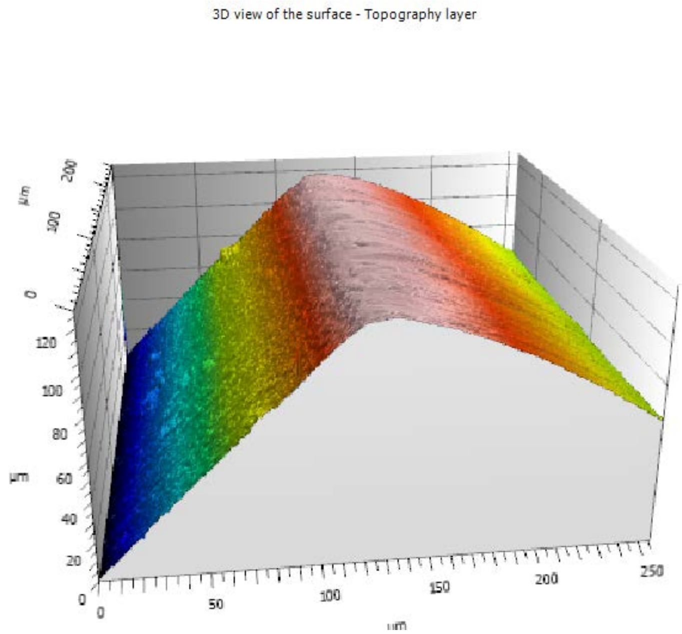

Figure 73: Trial 1- Unfinished Edge 3D View (MountainsMap)

1200 Grit Polish - There is still a curved side to one edge, however there is also a burr at the peak. This has an offset effect on the sides of the edges. The offset at this polish is at about 5µm. This irregularity is most likely due to polishing in the direction perpendicular to the edge tip.

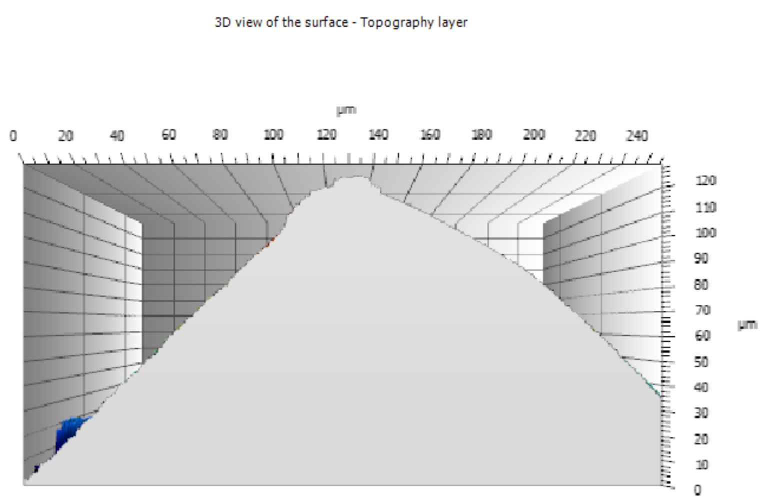

Figure 74: Trial 1- 1200 Grit Edge 2D View (MountainsMap)

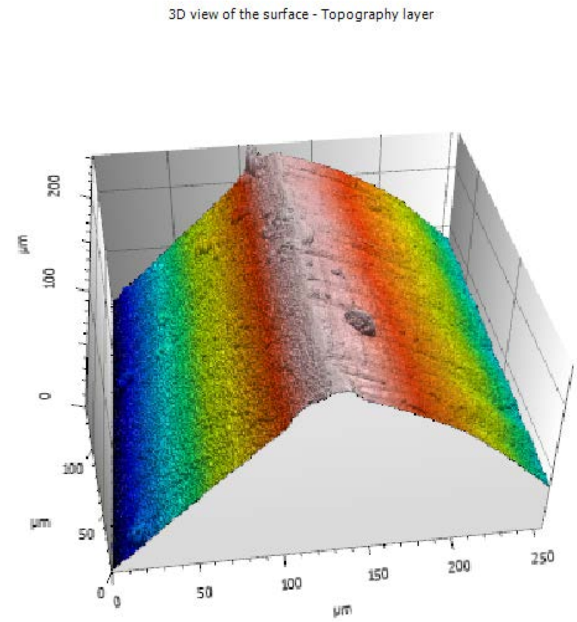

Figure 75: Trial 1- 1200 Grit Edge 3D View (MountainsMap)

2000 Grit Polish - With the finest polish we used, we found that the curved edge became much more linear, however the burr and offset at the peak became even worse. There is about a 10µm difference in height for the opposite sides of the edge.

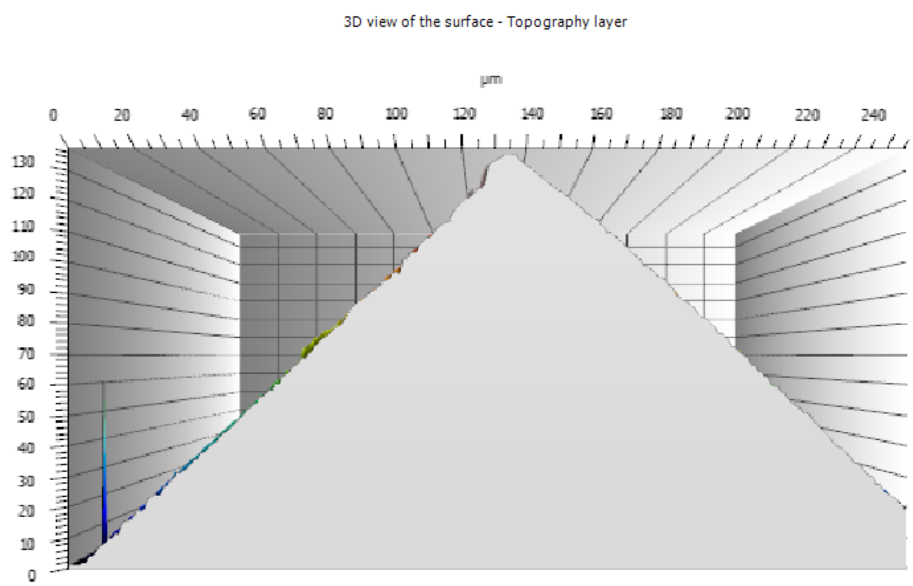

Figure 76: Trial 1- 2000 Grit Edge 2D View (MountainsMap)

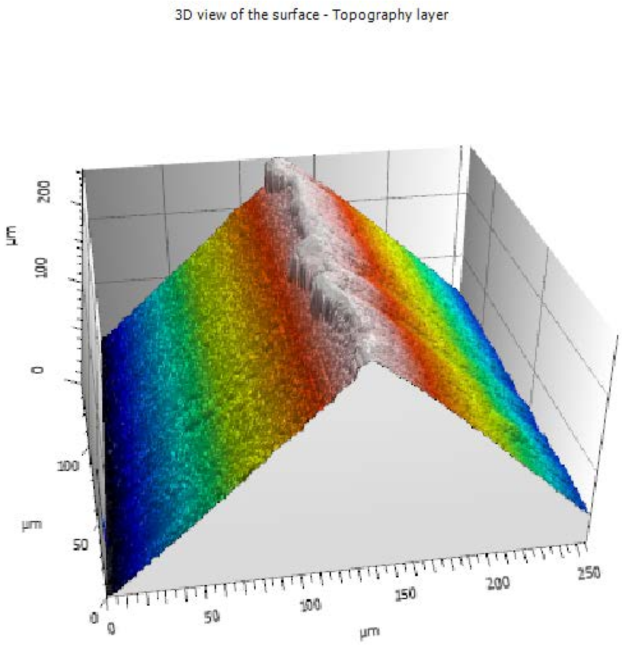

Figure 77: Trial 1- 2000 Grit Edge 3D View (MountainsMap)

Appendix D: Wax

The figures below are of each wax sample we used in the experiment. We ran three trials of each edge. Any outliers or noise within these measurements were eliminated using MountainsMap "Remove Outliers" operator. Some of the measurements have many outliers that could not be removed. This can skew the results when doing analyses because either the outliers are adding to the mathematical methods in a harmful way or there is data missing from the set. The following are figures of each of the trials that were not used for analysis in Section 3.3.

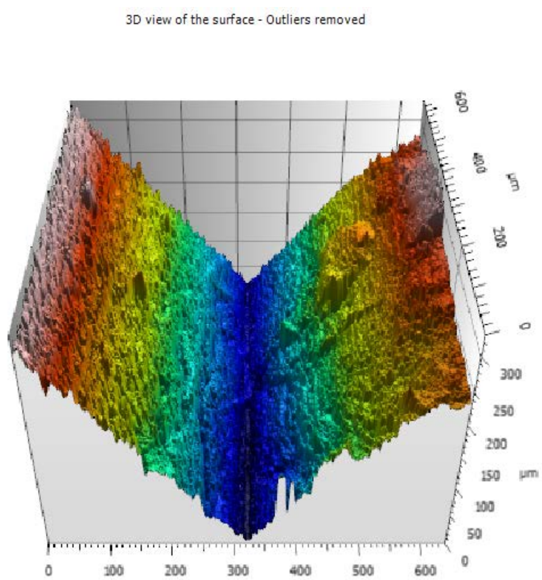

Figure 78: Unfinished Edge Trial 2 Wax (MountainsMap)

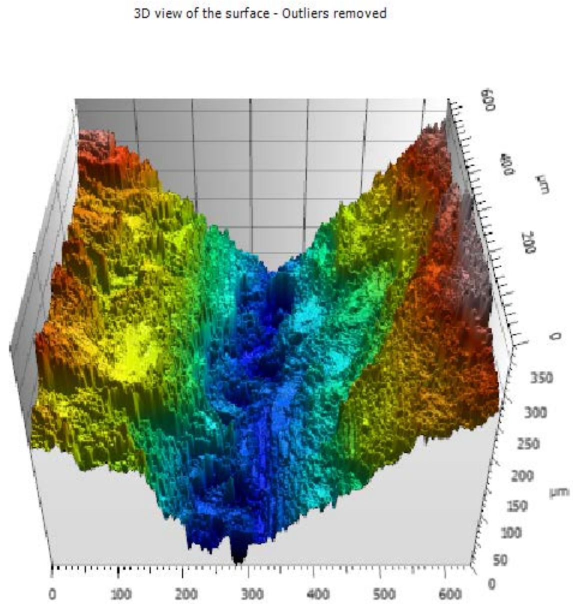

Figure 79: Unfinished Edge Trial 3 Wax (MountainsMap)

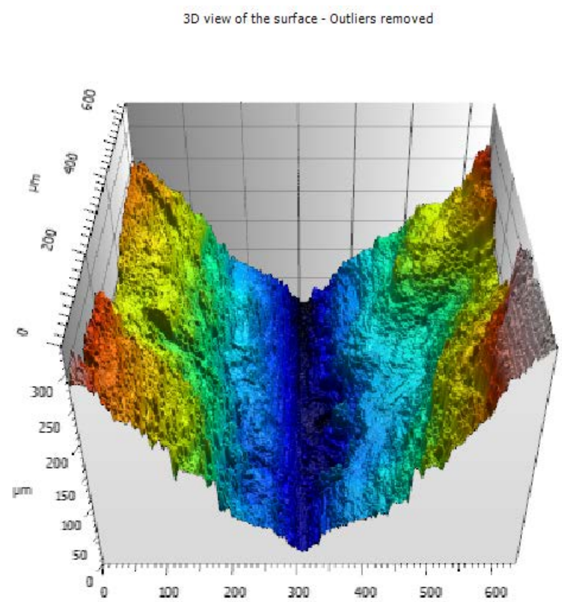

Figure 80: 1200 Grit Polished Edge Trial 2 Wax (MountainsMap)

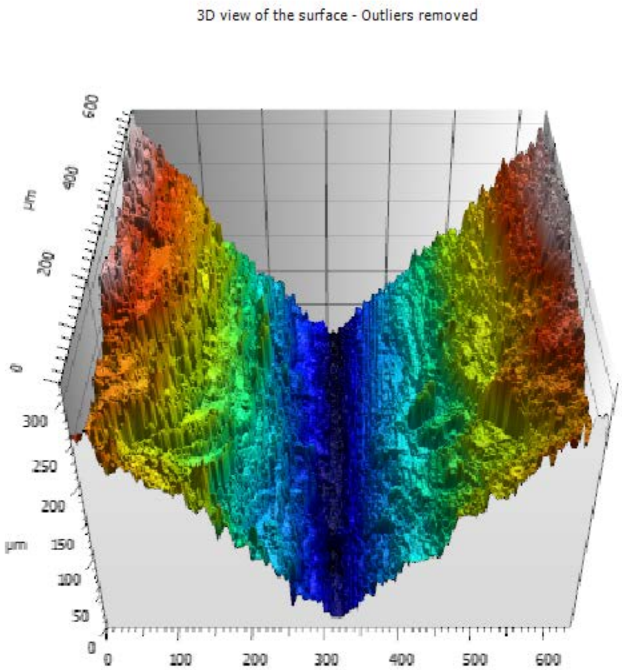

Figure 81: 1200 Grit Polished Edge Trial 3 Wax (MountainsMap)

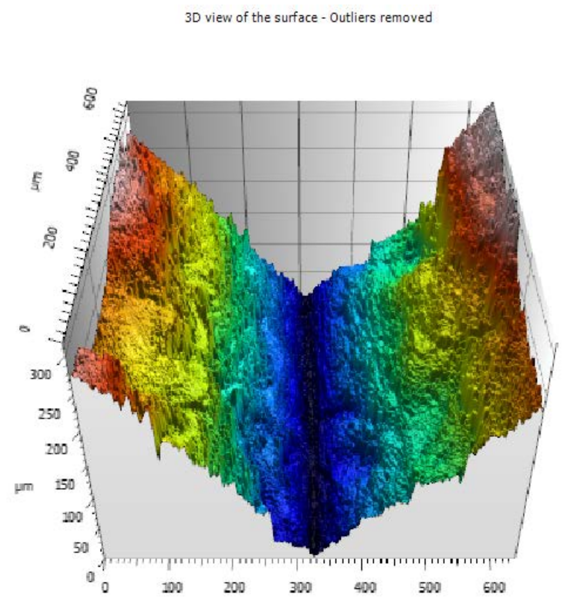

Figure 82: 1500 Grit Polished Edge Trial 1 Wax (MountainsMap)

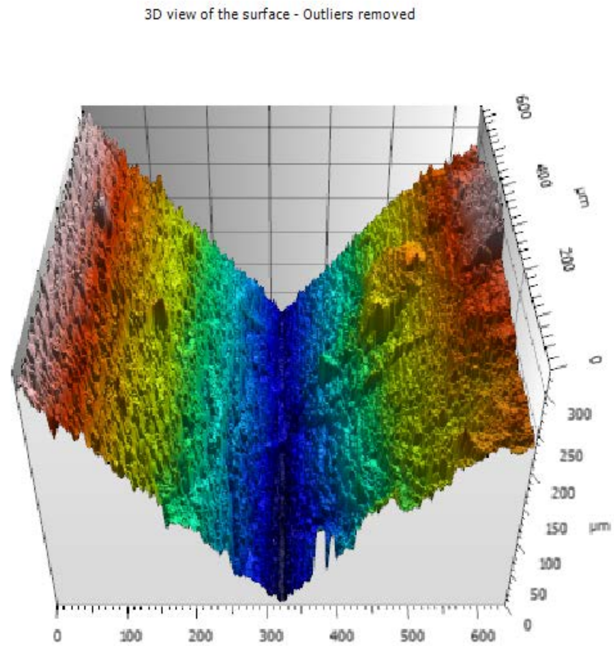

Figure 83: 1500 Grit Polished Edge Trial 2 Wax (MountainsMap)

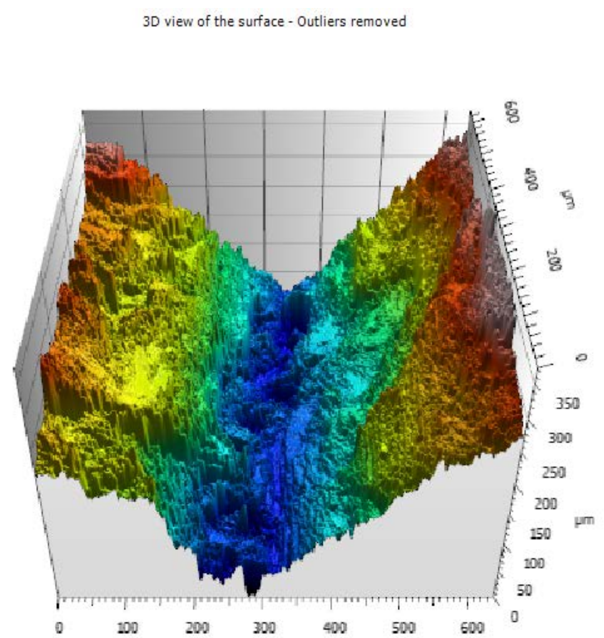

Figure 84: 1500 Grit Polished Edge Trial 3 Wax (MountainsMap)

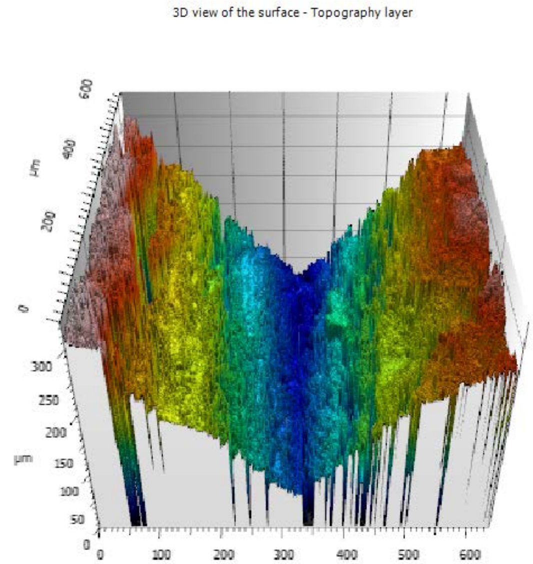

Figure 85: 2000 Grit Polished Edge Trial 1 Wax (MountainsMap)

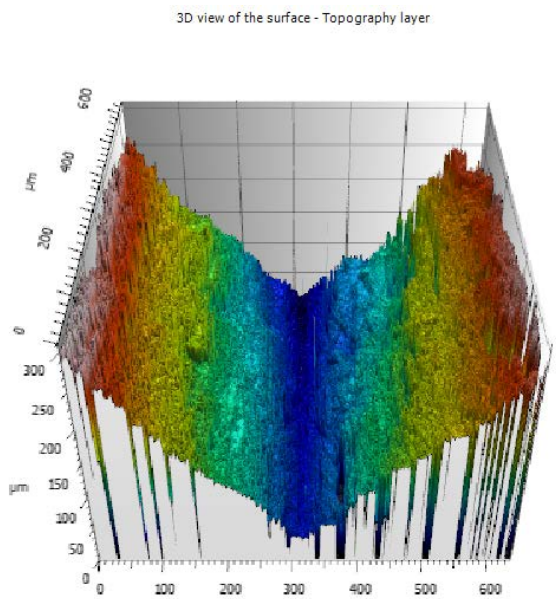

Figure 86: 2000 Grit Polished Edge Trial 2 Wax (MountainsMap)

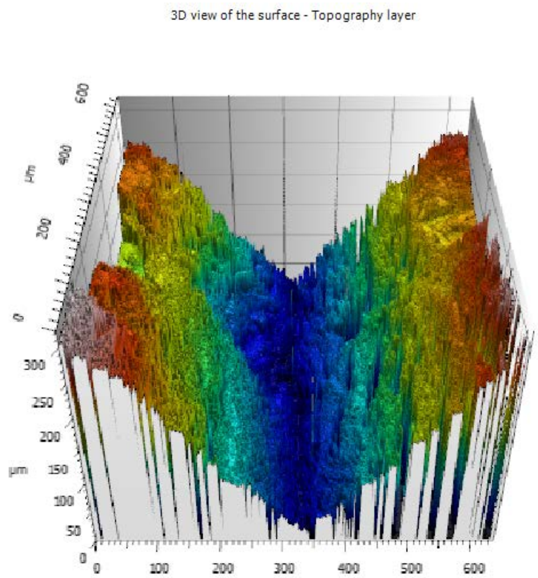

Figure 87: 2000 Grit Polished Edge Trial 3 Wax (MountainsMap)

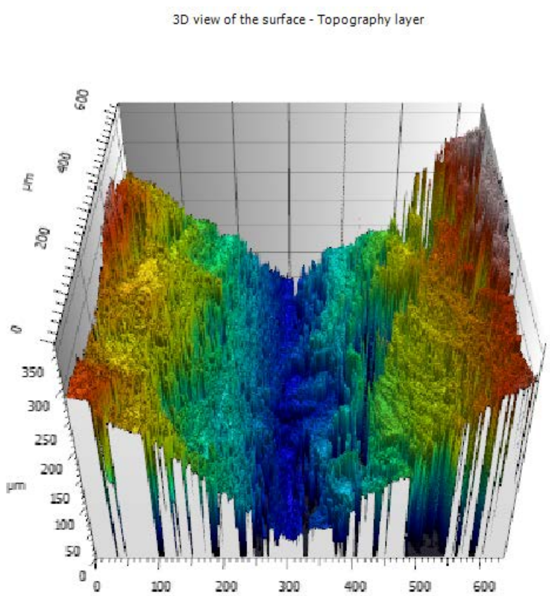

Figure 88: 3000 Grit Polished Edge Trial 1 Wax (MountainsMap)

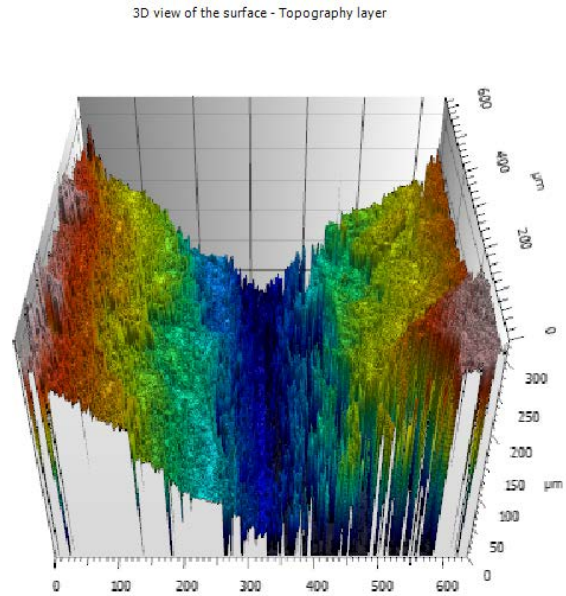

Figure 89: 3000 Grit Polished Edge Trial 2 Wax (MountainsMap)

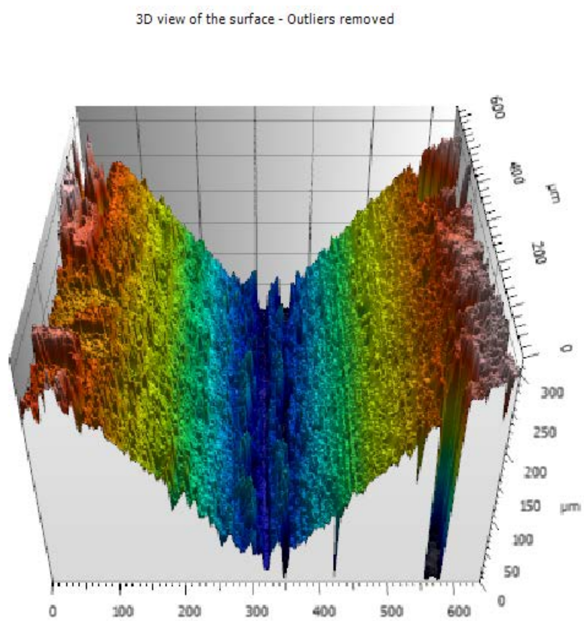

Figure 90: 3000 Grit Polished Edge Trial 3 Wax (MountainsMap)

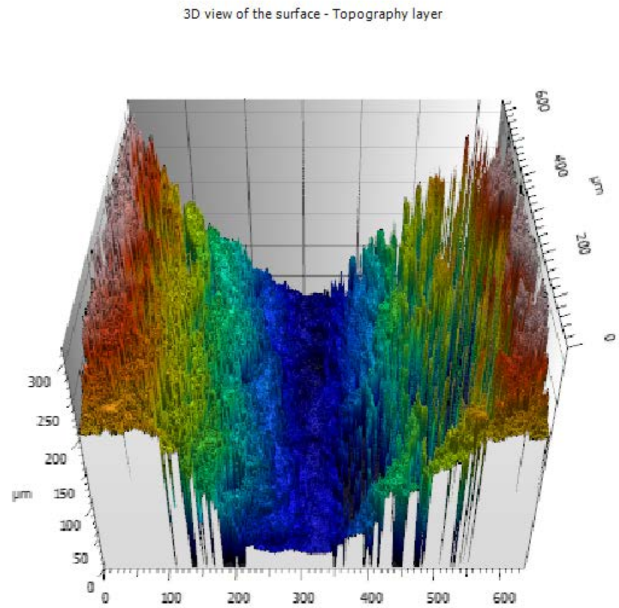

Figure 91: 2 Minute Mass Finished Edge Trial 1 Wax (MountainsMap)

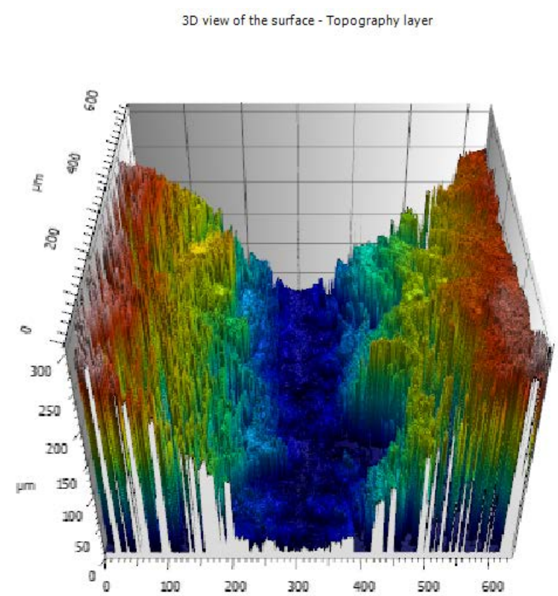

Figure 92: 2 Minute Mass Finished Edge Trial 2 Wax (MountainsMap)

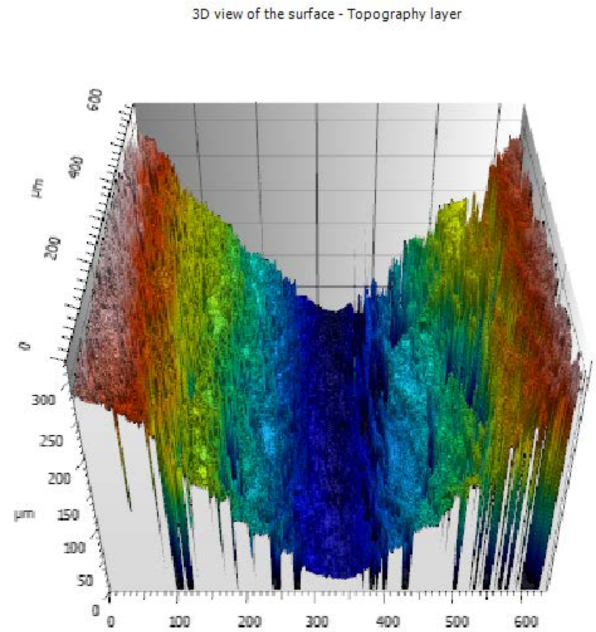

Figure 93: 4 Minute Mass Finished Edge Trial 1 Wax (MountainsMap)

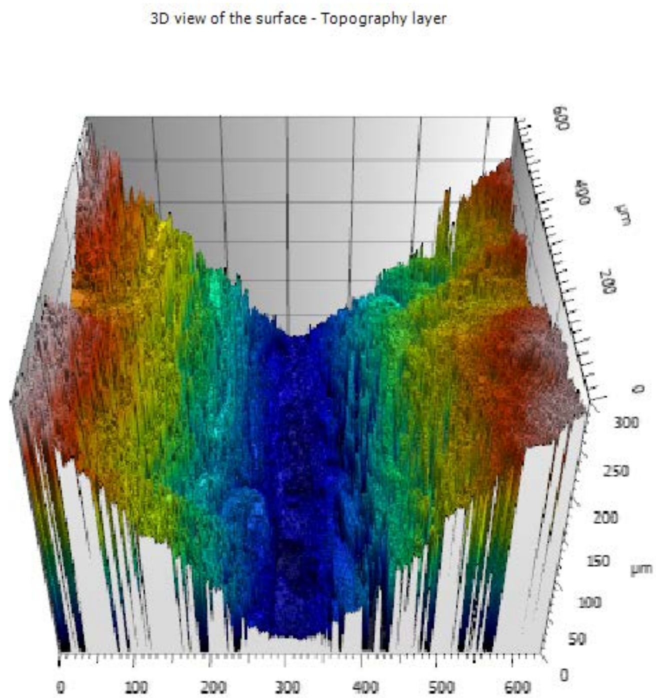

Figure 94: 4 Minute Mass Finished Edge Trial 2 Wax (MountainsMap)

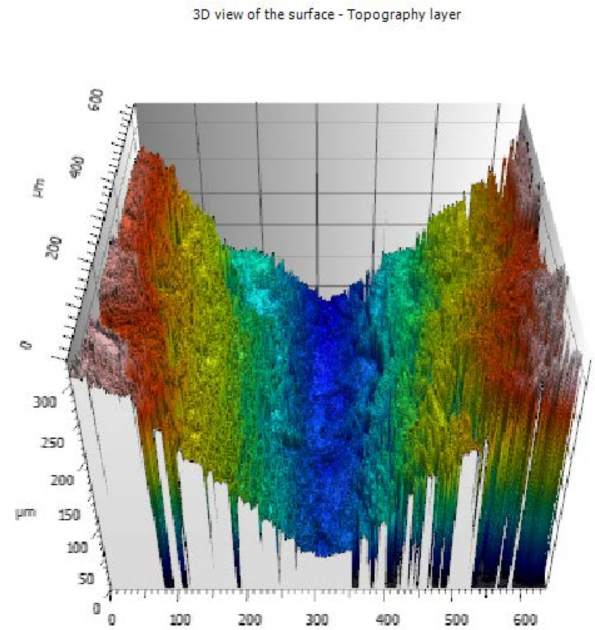

Figure 95: 4 Minute Mass Finished Edge Trial 3 Wax (MountainsMap)

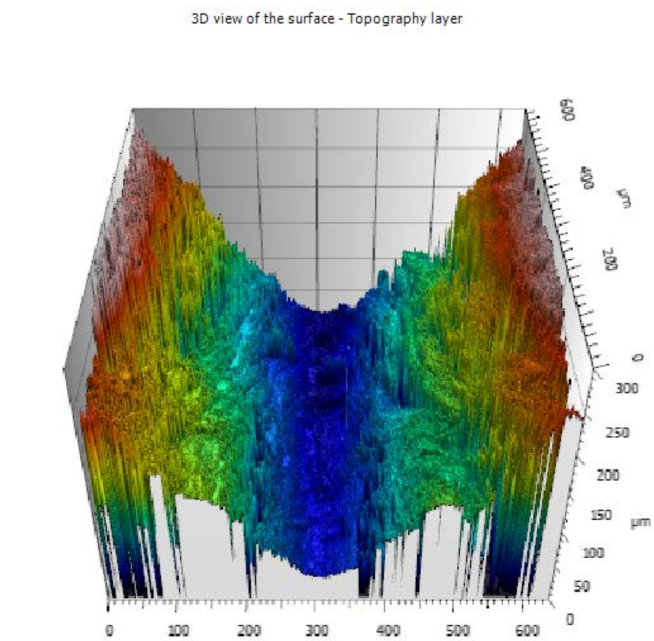

Figure 96: 8 Minute Mass Finished Edge Trial 1 Wax (MountainsMap)

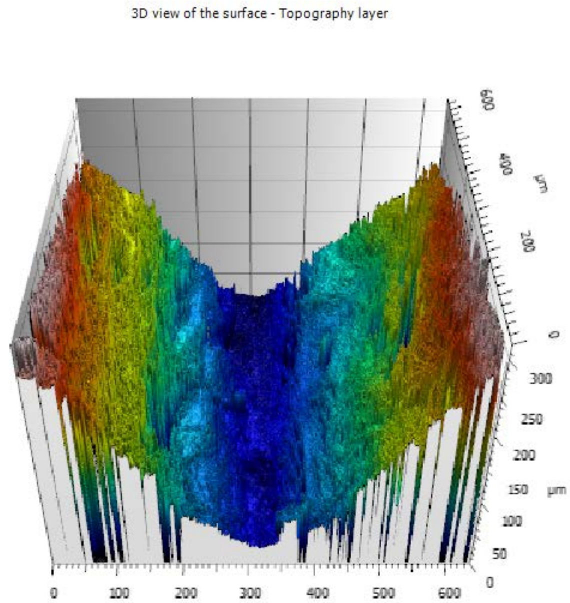

Figure 97: 8 Minute Mass Finished Edge Trial 2 Wax (MountainsMap)

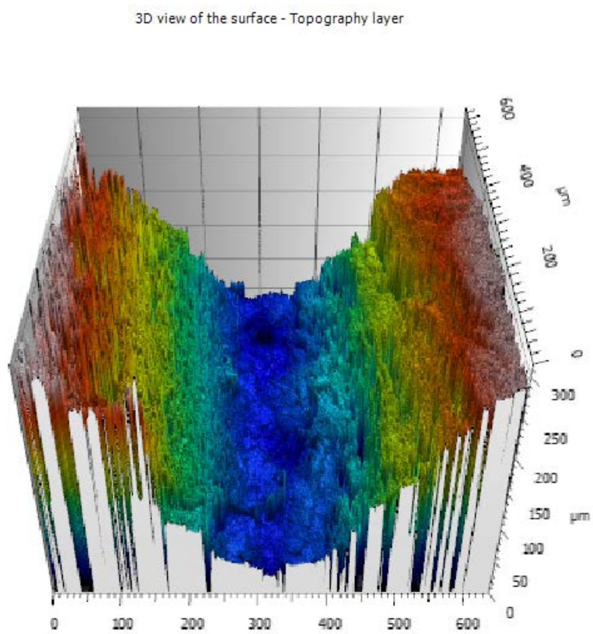

Figure 98: 8 Minute Mass Finished Edge Trial 3 Wax (MountainsMap)

Appendix E: Excel Force vs. Time Graphs

The figures below are Force vs. Time graphs for the remaining experiment trials that were not used for analysis in Section 3.1. These graphs were still observed for stick slip and maximum force for comparison to the trials used in Section 3.1.

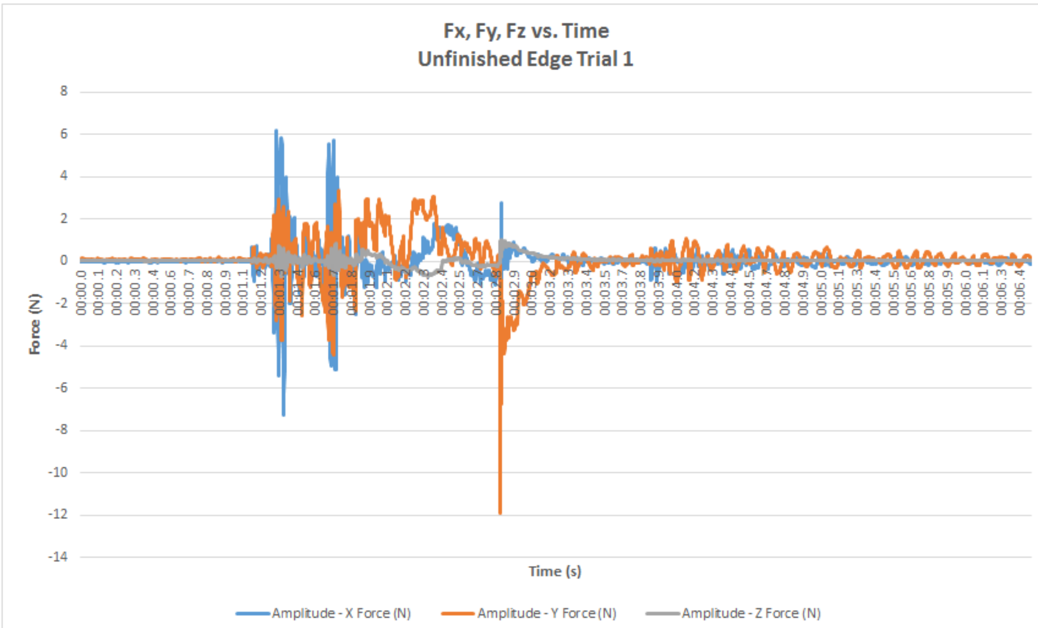

Figure 99: Force vs. Time- Unfinished Edge Trial 1 (Microsoft Excel)

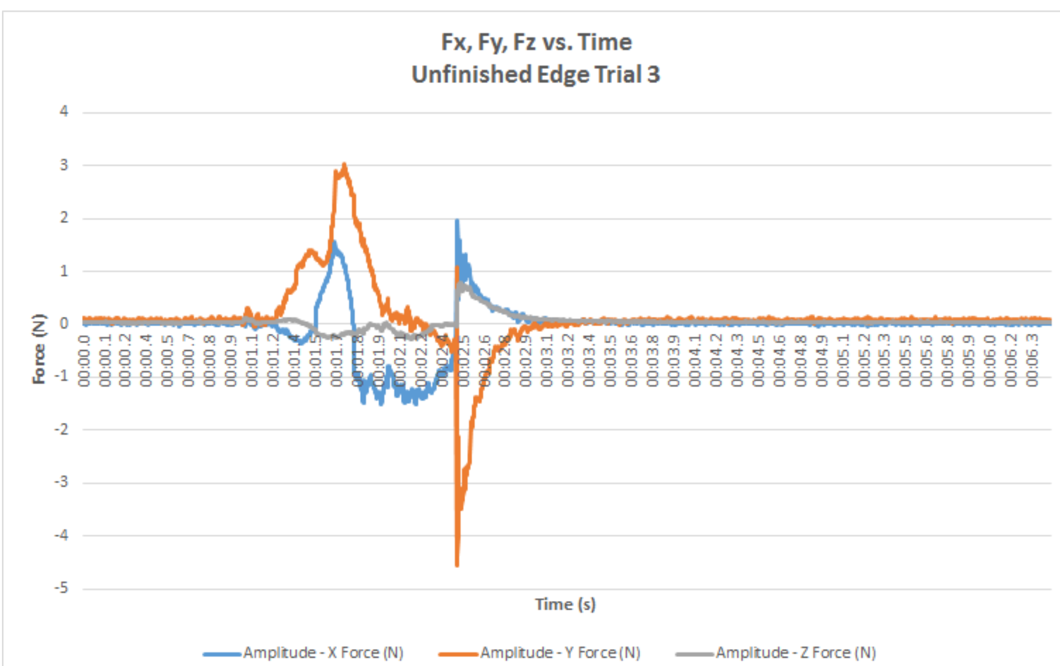

Figure 100: Force vs. Time- Unfinished Edge Trial 3 (Microsoft Excel)

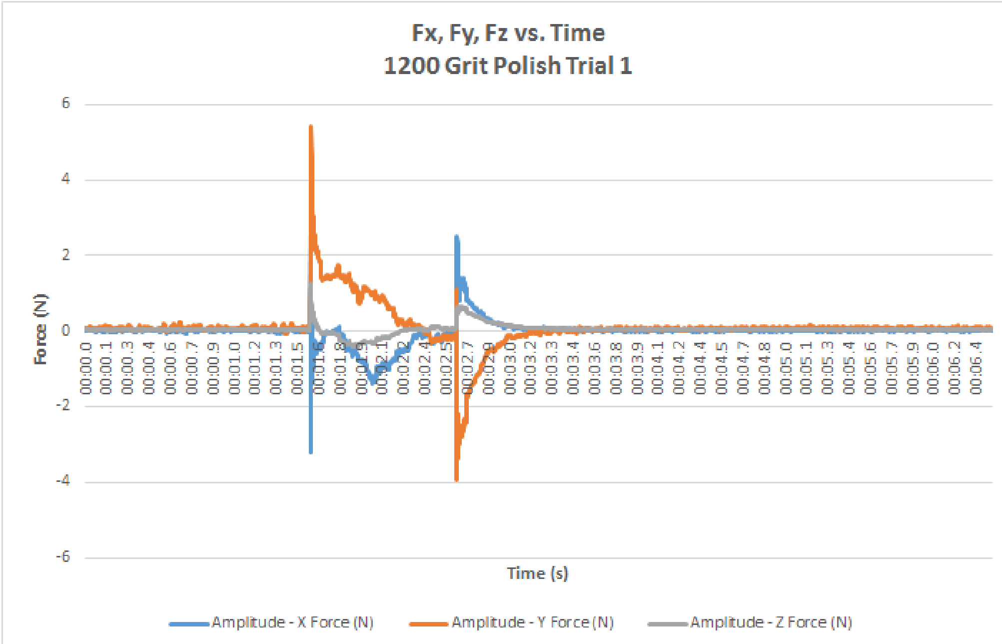

Figure 101: Force vs. Time- 1200 Grit Polished Edge Trial 1 (Microsoft Excel)

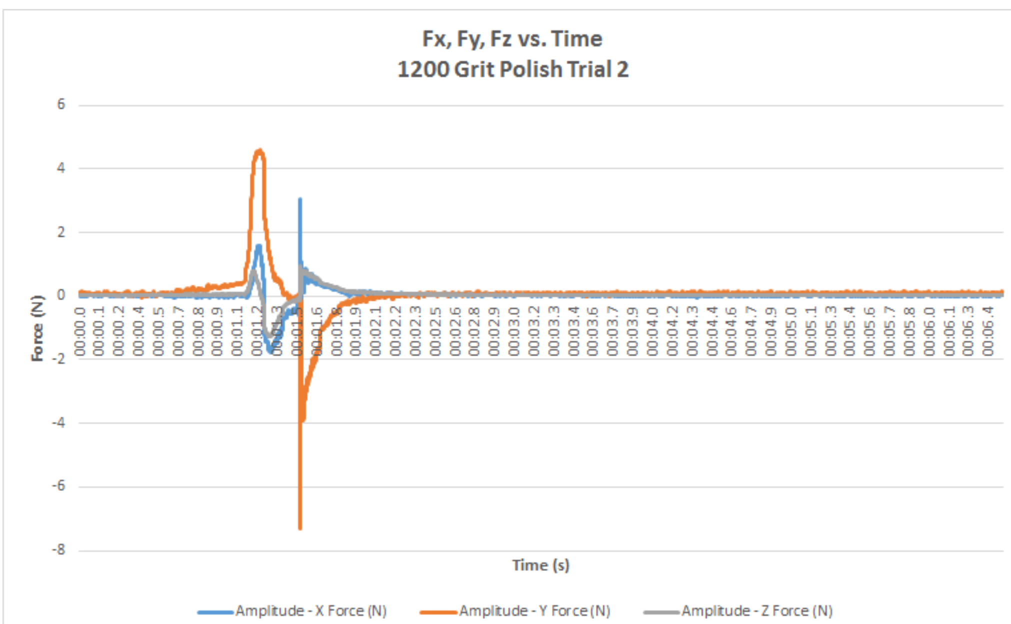

Figure 102: Force vs. Time- 1200 Grit Polished Edge Trial 2 (Microsoft Excel)

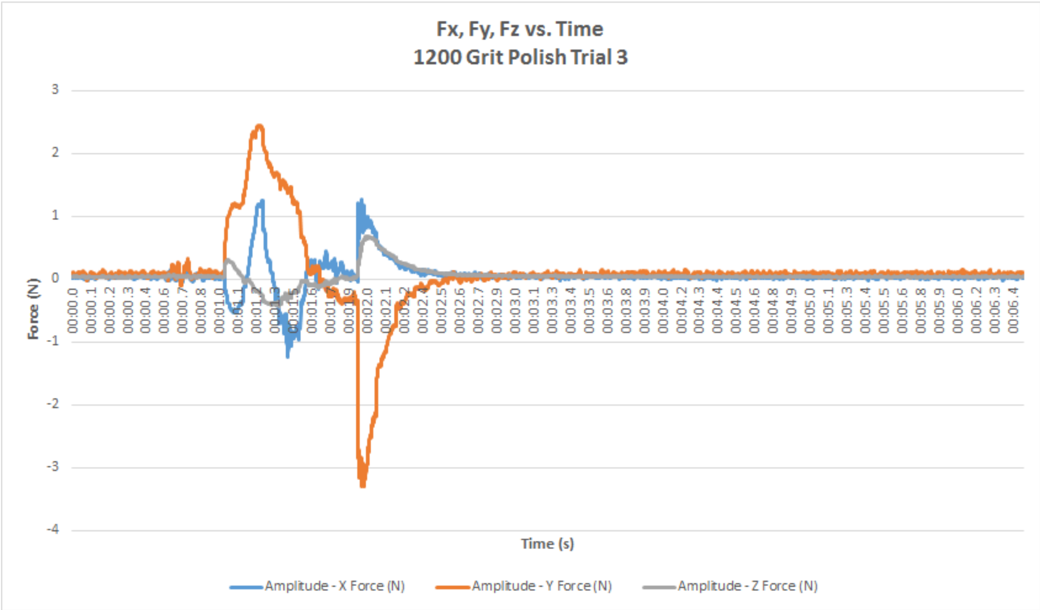

Figure 103: Force vs. Time- 1200 Grit Polished Edge Trial 3 (Microsoft Excel)

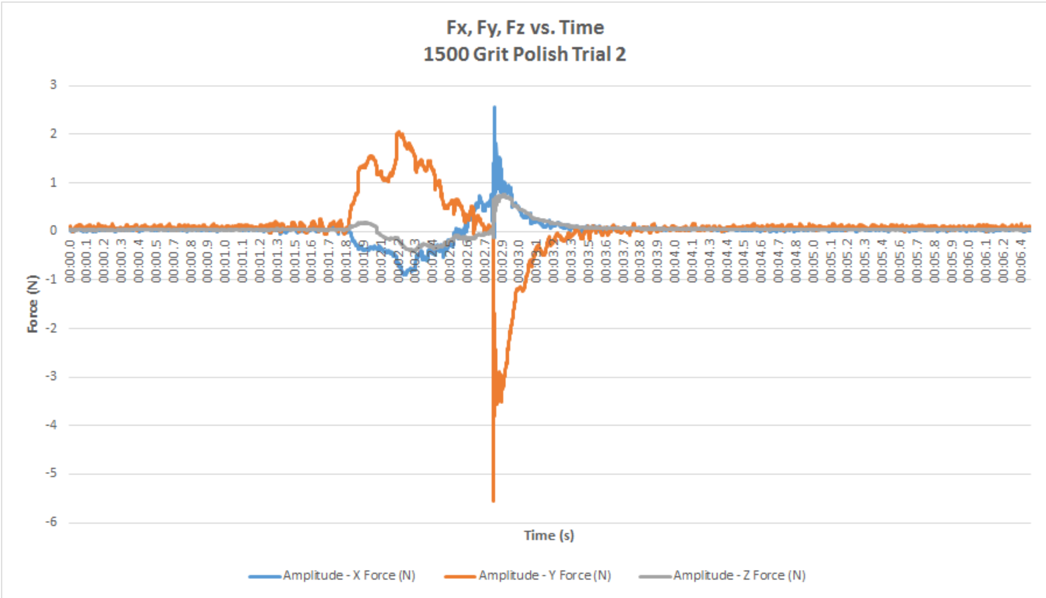

Figure 104: Force vs. Time- 1500 Grit Polished Edge Trial 2 (Microsoft Excel)

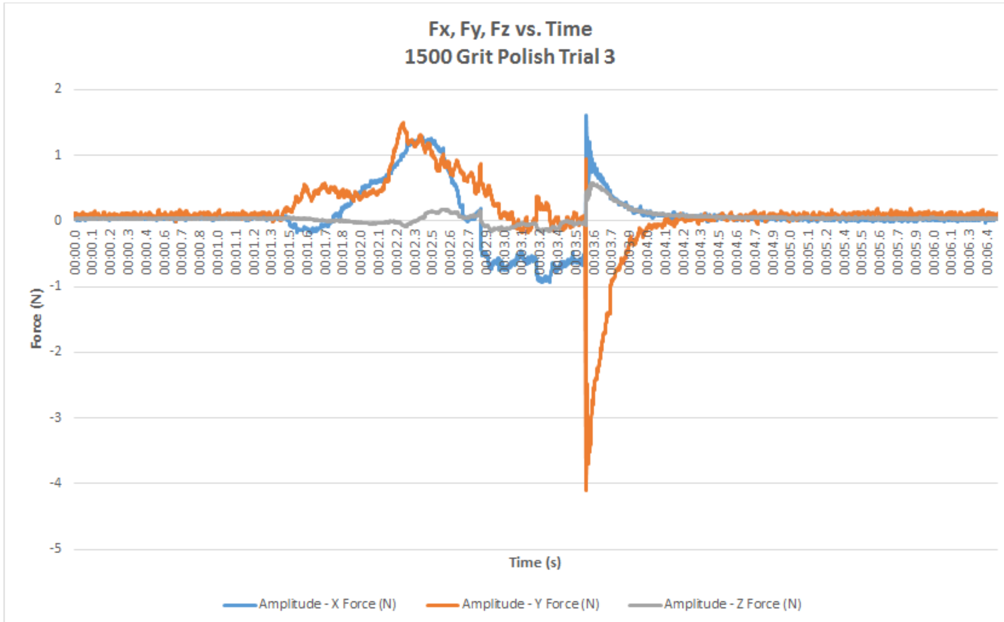

Figure 105: Force vs. Time- 1500 Grit Polished Edge Trial 3 (Microsoft Excel)

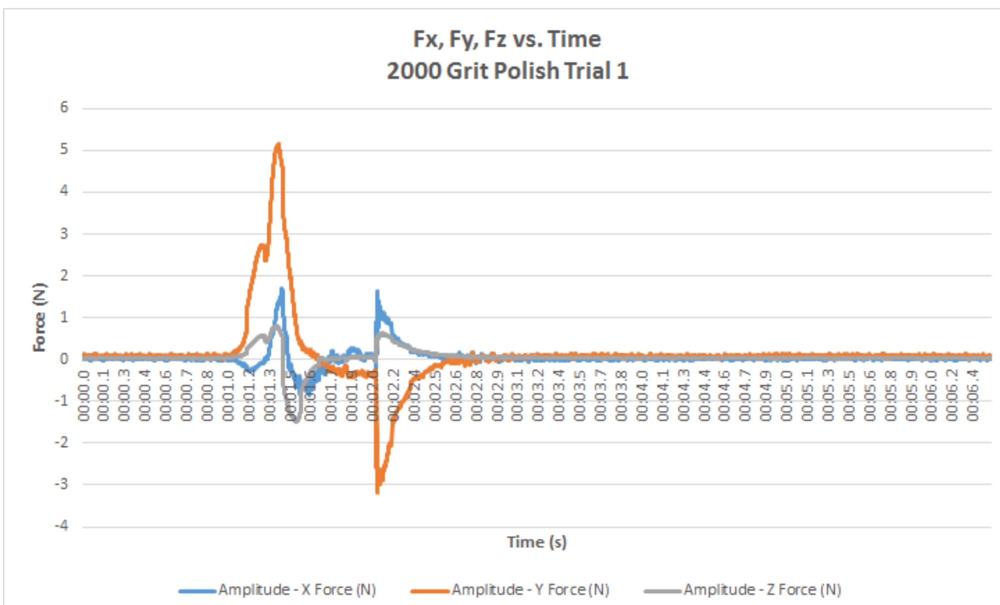

Figure 106: Force vs. Time- 2000 Grit Polished Edge Trial 1 (Microsoft Excel)

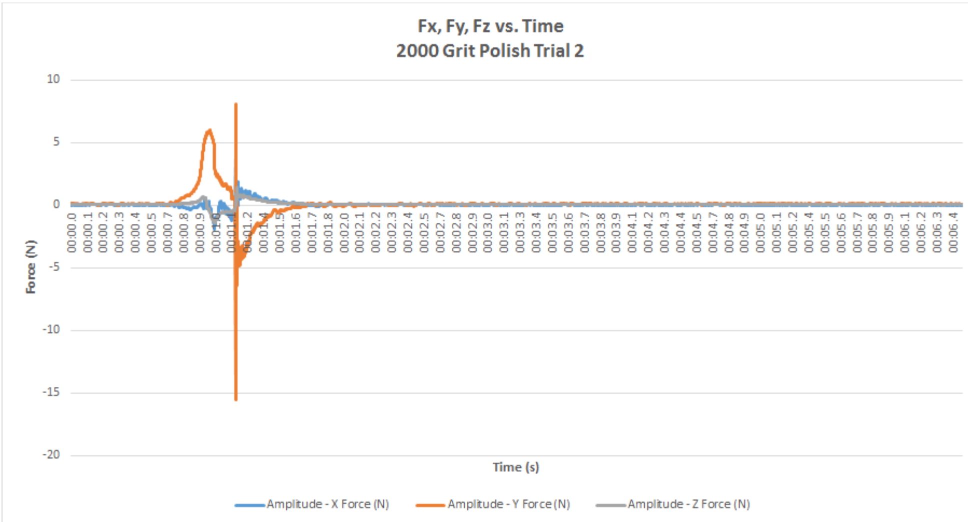

Figure 107: Force vs. Time- 2000 Grit Polished Edge Trial 2 (Microsoft Excel)

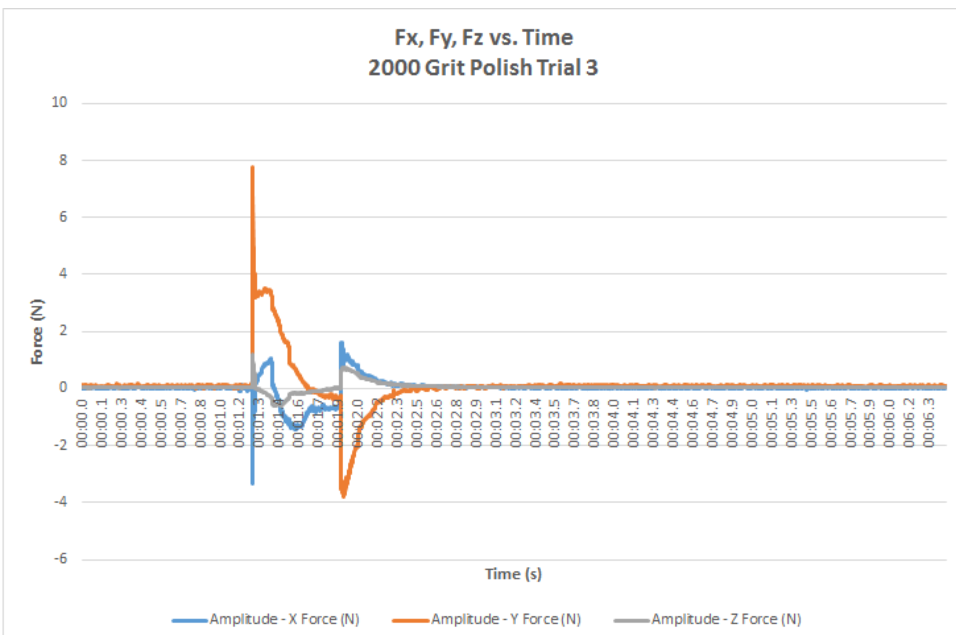

Figure 108: Force vs. Time- 2000 Grit Polished Edge Trial 3 (Microsoft Excel)

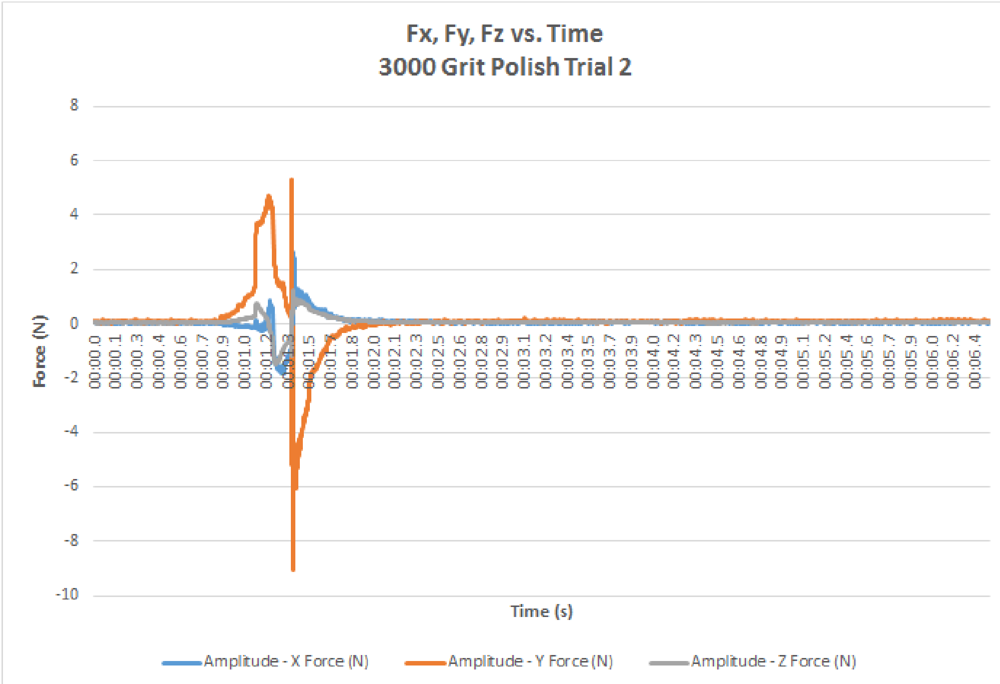

Figure 109: Force vs. Time- 3000 Grit Polished Edge Trial 2 (Microsoft Excel)

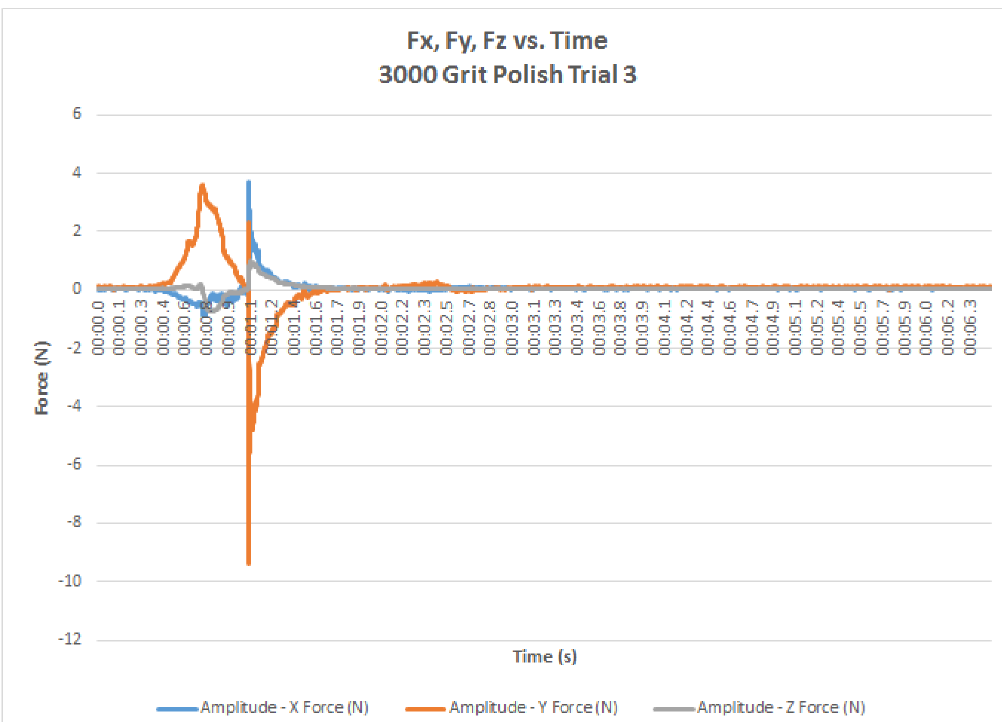

Figure 110: Force vs. Time- 3000 Grit Polished Edge Trial 3 (Microsoft Excel)

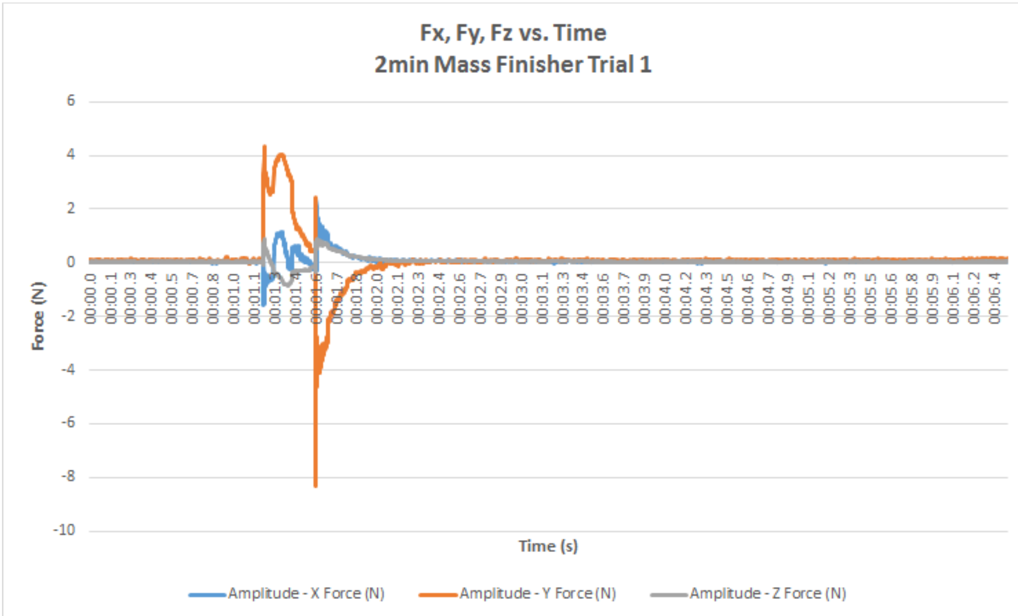

Figure 111: Force vs. Time- 2 Minute Mass Finished Edge Trial 1 (Microsoft Excel)

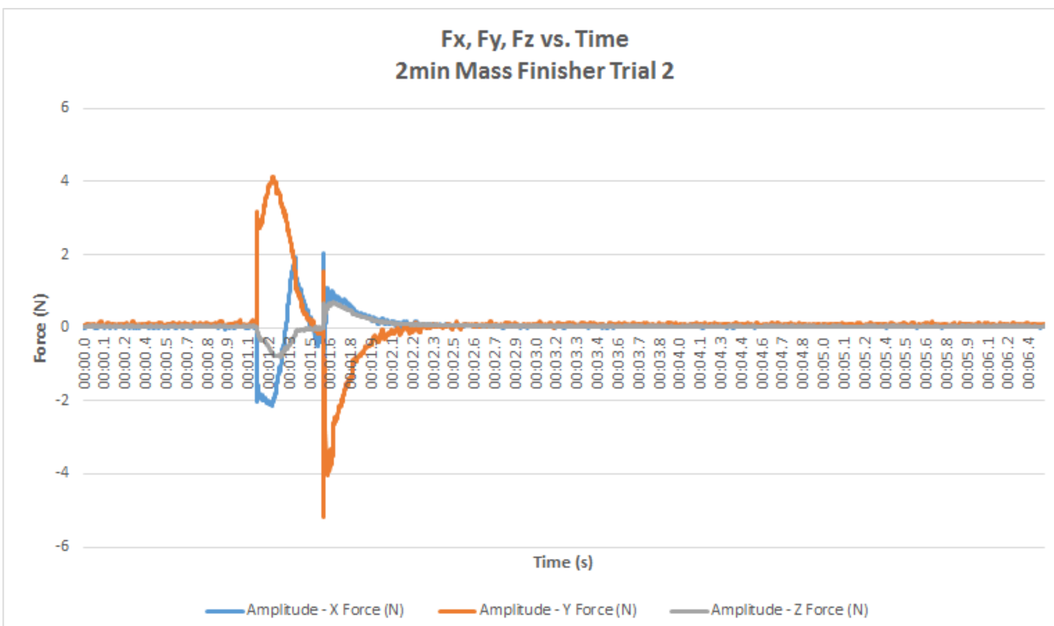

Figure 112: Force vs. Time- 2 Minute Mass Finished Edge Trial 2 (Microsoft Excel)

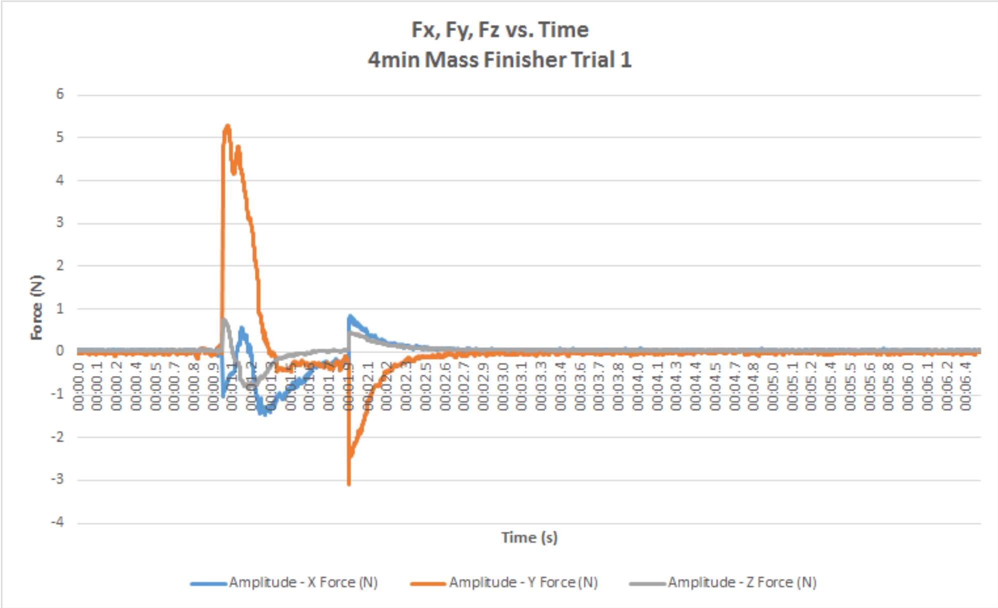

Figure 113: Force vs. Time- 4 Minute Mass Finished Edge Trial 1 (Microsoft Excel)

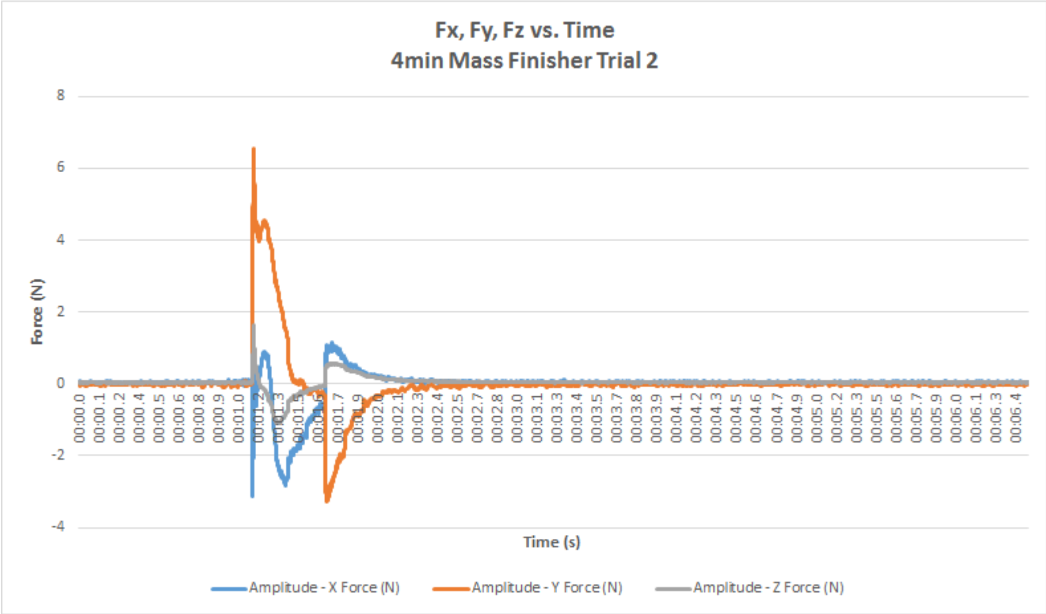

Figure 114: Force vs. Time- 4 Minute Mass Finished Edge Trial 2 (Microsoft Excel)

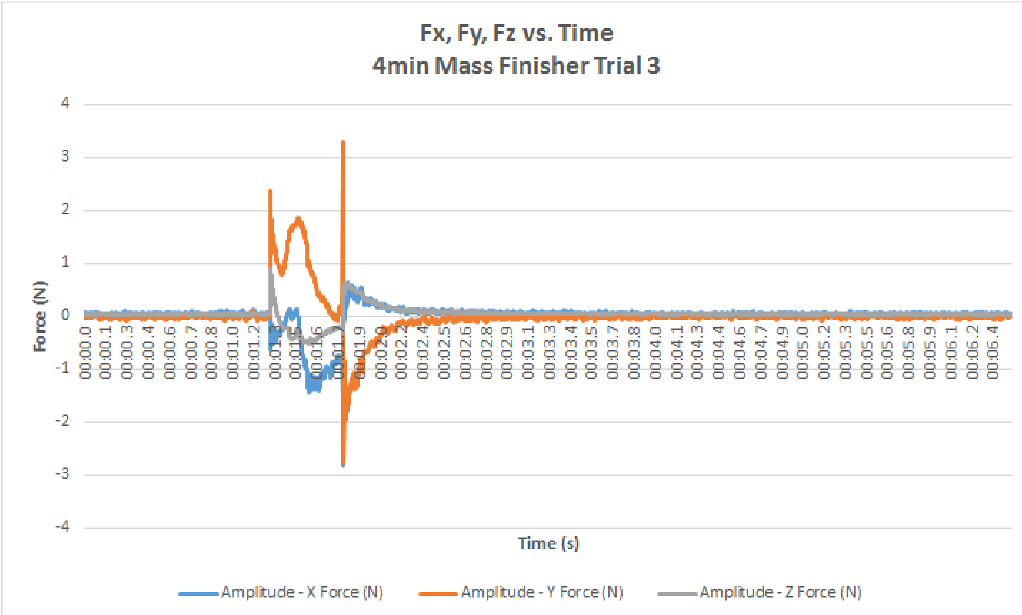

Figure 115: Force vs. Time- 4 Minute Mass Finished Edge Trial 3 (Microsoft Excel)

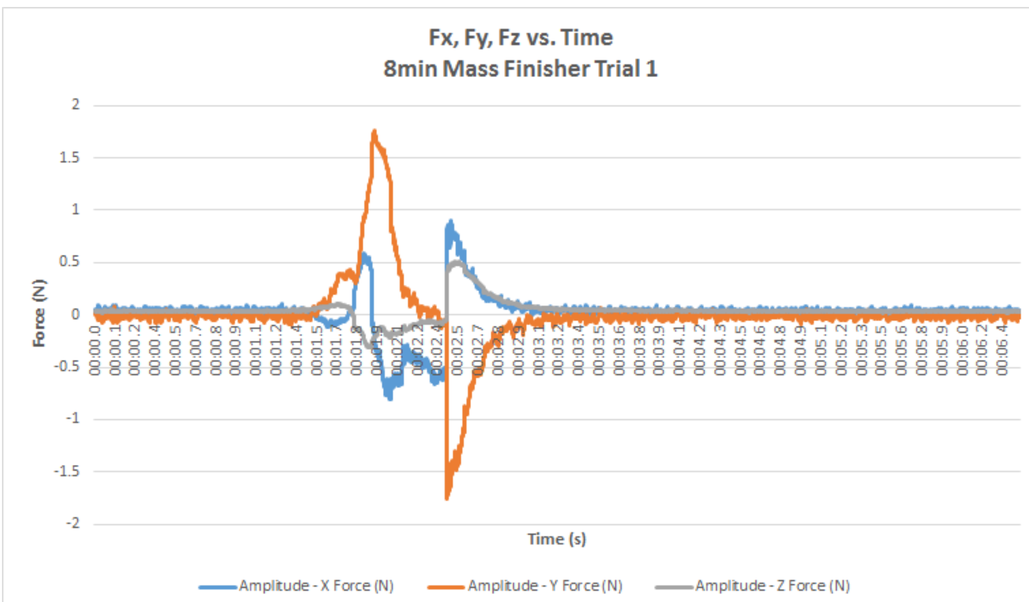

Figure 116: Force vs. Time- 8 Minute Mass Finished Edge Trial 1 (Microsoft Excel)

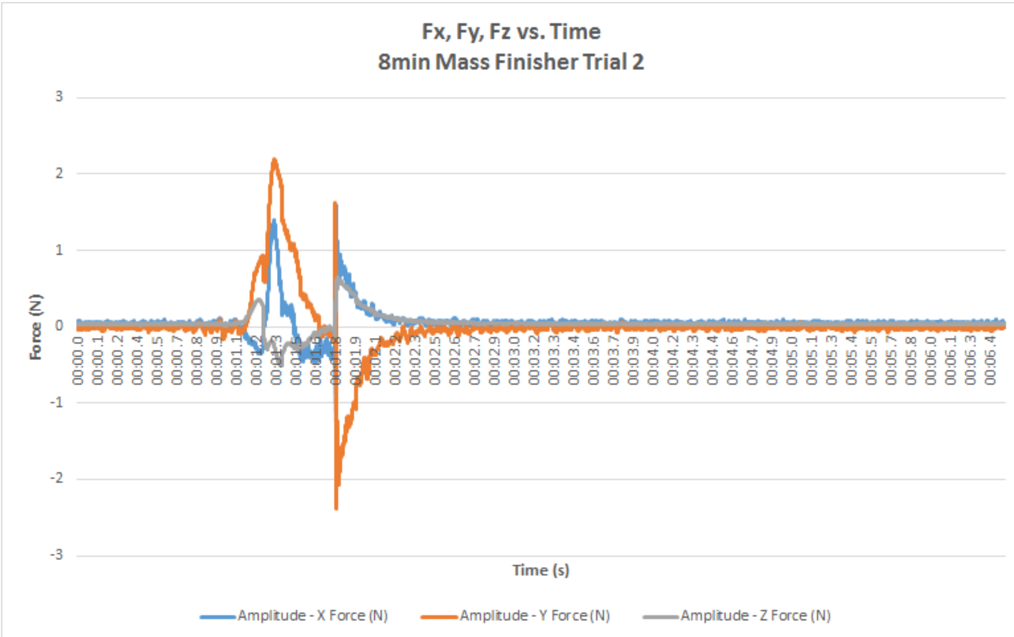

Figure 117: Force vs. Time- 8 Minute Mass Finished Edge Trial 2 (Microsoft Excel)

Appendix F: LabVIEW VI

Below are figures of the front panel and block diagram from our LabVIEW script, which was developed for data acquisition.

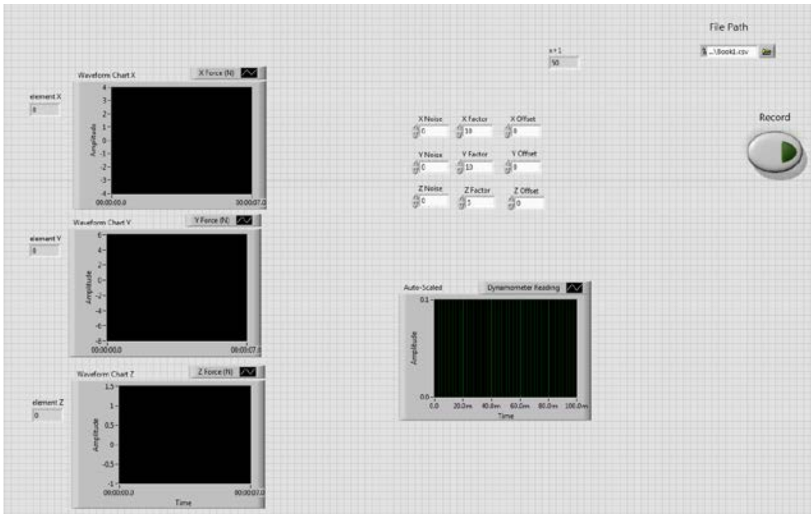

Figure 118: LabVIEW VI- Front Panel (LabVIEW)

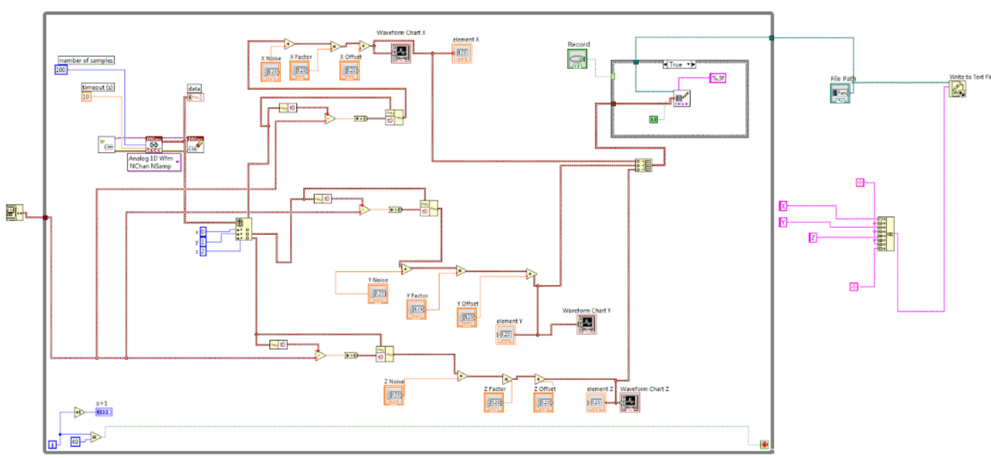

Figure 119: LabVIEW VI- Block Diagram (LabVIEW)

Appendix G: Razor Blades

Our initial plan for material selection was to use precision slicing blades and box-cutting blades for testing. The tip radii of these blades are extremely fine, and can be difficult to measure using the Olympus microscope. Because it was difficult to measure the blades, we pivoted the project to using aluminum edges for testing. These aluminum edges have tip radii that are 90 degrees, which are much easier to measure using the Olympus microscope. The aluminum edges still relate to a wide variety of slicing applications and were suitable for this project.

Figure 120: Razor Blades Initially Used for Testing

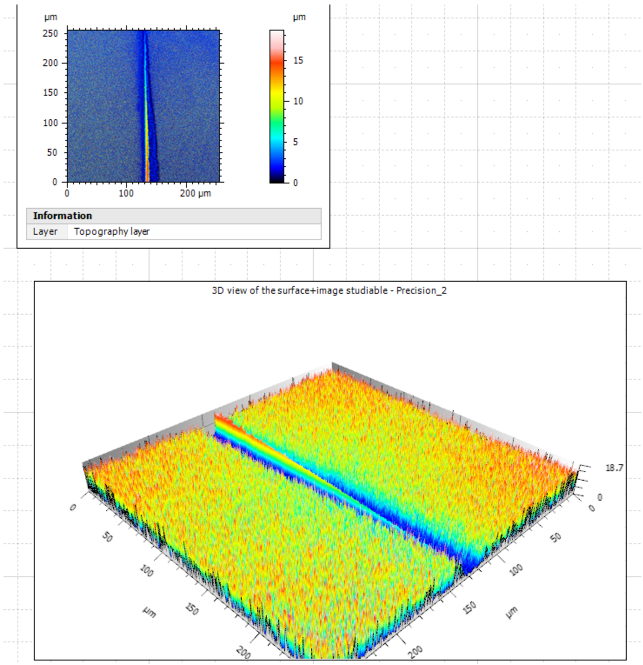

Figure 121: MountainsMap Precision Blade Analysis (MountainsMap)